INFORMATION TO USERS

This manuscript has been reproduced from the microfilm master. UMI films the text directly from the original or copy submitted. Thus, some thesis and dissertation copies are in typewriter face, while others may be from any type of computer printer.

The quality of this reproduction is dependent upon the quality of the copy submitted. Broken or indistinct print, colored or poor quality illustrations and photographs, print bleedthrough, substandard margins, and improper alignment can adversely affect reproduction.

In the unlikely event that the author did not send UMI a complete manuscript and there are missing pages, these will be noted. Also, if unauthorized copyright material had to be removed, a note will indicate the deletion.

Oversize materials (e.g., maps, drawings, charts) are reproduced by sectioning the original, beginning at the upper left-hand corner and continuing from left to right in equal sections with small overlaps.

ProQuest Information and Learning
300 North Zeeb Road, Ann Arbor, MI 48106-1346 USA
800-521-0600

SC

LAMINAR FLOW OF POLYMER SOLUTIONS

AT HIGH SHEAR RATES

by

SATYA NARAIN PASARI

A THESIS SUBMITTED IN PARTIAL FULFILMENT OF

THE REQUIREMENT FOR THE DEGREE OF

MASTER OF APPLIED SCIENCE

in the

DEPARTMENT OF CHEMICAL ENGINEERING

UNIVERSITY OF OTTAWA

Ottawa, Canada

February, '69

W. Korjchi

Research Director

Satya Narain Pasari

Candidate

ABSTRACT

The theory of steady, laminar, one-dimensional Poiseuille flow of high molecular weight polymers in aqueous solutions is presented for the general case of the fluid exhibiting anomalous surface effects at the solid wall. A capillary viscometer was used to determine the rheological properties over intermediate and high shear rates. Polymer adsorption and separation phenomena account for the different flow curves obtained for various calillary diameters. A mathematical model correlated the experimental data and explained the polymer behavior. The analysis showed the importance of capillary diameter and applied shear stress in explaining the anomalous flow behavior.

ACKNOWLEDGEMENT

The author is indebted to Dr. William Kozicki for his guidance and constant encouragement in carrying out this work. Further, he wishes to express his gratitude to Dr. Carlos Tiu and Mr. A.R.K. Rao for their assistance from time to time.

Appreciation is also extended to Mr. G. Gasperetti for his willing assistance in the construction of equipment.

TABLE OF CONTENTS

LIST OF FIGURES

CHAPTER I

INTRODUCTION

The behavior of high molecular weight polymers in solutions and melts has been studied extensively for many scientific and engineering applications. When used as additive, the physico-chemical properties of polymer molecules affect the viscometric characteristics of the mineral oils. Polymers have also received extensive use in thickening hydraulic fluids and lubricants. Certain areas of polymer behavior are complex and controversy exists concerning the nature of these complex systems. Nevertheless, the viscometry of polymer solutions has contributed substantially to the understanding of the physical characteristics of macromolecules.

The purpose of present work was to develop theoretical relationships for the general case of polymer fluids exhibiting anomalous flow behavior near the solid surface. The physical phenomena observed for aqueous Natrosol solutions are best explained in the light of a slip phenomenon. The study was conducted over intermediate and high shear rates. Following assumptions were made:

(1) Steady, one dimensional laminar flow takes place. Hence, visco-elasticity has no effect whatsoever on the flow pattern and the shear stress is a unique although unspecified function of the shear rate.

(2) The effective velocity of slip at the solid surface is either zero or some finite positive or negative value, U_W.

CHAPTER II

RHEOLOGY OF NON-NEWTONIAN MATERIALS

The discovery by Bingham and Green (5) in 1919 that oil paint is a plastic solid and not a liquid gave birth to the science of modern rheology. Since then, Rheology as "the science of flow and deformation of matter" has progressed steadily. The primary aim of rheology has been to formulate constitutive equations capable of describing many observed phenomena on various fluids of interest to engineers. The failure to exhibit Newtonian properties, i.e. strict proportionality between stress and strain rate, by high viscosity liquids, polymers, colloids, sols, gels, concentrated slurries, biological fluids, solutions of macromolecules etc. has necessitated the formulation of many constitutive equations and rheological models.

A. Generalized Newtonian Fluids

A most useful and practical constitutive equation is provided by the "generalized Newtonian Model" (43).

$$\overset{\rightrightarrows}{\tau} = -\eta\,(II)\overset{\rightrightarrows}{\Delta} \qquad \text{..... (A-1)}$$

where η is a function of the second invariant of the rate of strain tensor. This invariant can be expressed as a function of the following scalar invariants:

$$II = (\vec{\Delta}:\vec{\Delta}) = \Sigma i\ \Sigma j\ \Delta ij\ \Delta ji \quad \ldots\ldots\ldots\ldots (A\text{-}2)$$

The equation (A-1) describes a viscous incompressible fluid for which the effects of cross viscosity and of the third invariant are not taken into consideration.

B. Other Rheological Models:

It is desirable that any proposed rheological model should represent the actual behavior of a fluid with accuracy in low as well as high shear rates. Bogue and Doughty (7) have listed a number of desirable properties of a theory to adequately describe the behavior of rheological materials. The theory should

(1) be co-ordinate invariant,

(2) predict shear dependent viscosities,

(3) predict normal stresses in steady shear,

(4) reconcile the dynamic experiments of linear viscoelasticity,

(5) explain stress-relaxation phenomenon and

(6) be explicit, with definite constants to be fitted to experimental data.

It is, however, difficult to formulate one constitutive equation capable of describing all the fluid properties. So, non-Newtonian fluids are classified into various categories. Pseudoplastics are the commonest non-Newtonian fluids. There are several useful constitutive equations (6) for pseudoplastics, even though they are not universally applicable. The

most common one that is widely used is the Power law (Ostwald-de Waele) model:

$$\tau_{ij} = - \{ m \left(\tfrac{1}{2} II\right)^{\frac{n-1}{2}} \} \Delta_{ij} \quad \ldots\ldots\ldots\ldots\ldots \text{(B-1)}$$

where m and n are two positive fluid-parameters determinable from viscometric measurements. This simple equation fits the flow curves of almost all pseudoplastic materials over at least one decade of shear rate and also fits many commercially important polymeric materials over shear rate ranges up to three or four decades. This model, however, does not describe either the lower limiting viscosity or the upper limiting viscosity. Recently, a four constant model in which there are both, a lower limiting viscosity and an upper limiting viscosity, has been proposed by Meter (33,34):

$$\tau_{ij} = - \{ \eta_\infty + \frac{\eta_0 - \eta_\infty}{1 + \left(\frac{\sqrt{\frac{1}{2} II_\tau^*}}{\tau_m}\right)^q} \} \Delta_{ij} \quad \ldots\ldots\ldots \text{(B-2)}$$

where η_0, η_∞, q and τ_m are the fluid parameters.

C. Models for Viscoelastic Materials:

In the previous section, discussion was limited to those fluids which could be characterized by a knowledge of the

* $II_\tau \doteq \Sigma_i \Sigma_j \tau_{ij} \tau_{ji}$.

state of stress in a fluid and the relationship between stress and rate of strain. For many fluids such a characterization is not possible. The behavior of many fluids at a given instant of time depends not only on the state of stress but also on the way in which the stress and rate of strain are changing with time. The viscoelastic nature of a fluid is also important in viscometric flow. Here it produces "normal stress" effects.

In attempting to solve the problem of elastic response in many fluids, several theories of viscoelasticity have resulted. Viscoelastic theories due to Oldroyd (40), Rivlin and Ericksen (44), Noll (38), Coleman and Noll (13), Green and Rivlin (22), Ericksen (17) etc. have received considerable attention. The treatment by Oldroyd is the only one to have received significant engineering application. Recently Spriggs and Bird (50) have proposed a model capable of giving a reasonable description of non-Newtonian viscosity and normal stresses. This model includes some results from molecular theories (45, 57) to provide a link with the structural aspects of polymer solutions. More recently, Carreau and Bird (11) have proposed a rheological model for polymeric fluids. This model can describe non-Newtonian viscosity, shear-rate-dependent normal stresses, frequency-dependent complex viscosity, stress-relaxation after large-deformation flow, recoil and hysteresis loops. Their model takes the form:

$$\overset{\rightrightarrows}{\tau} = - \{\eta - \frac{D\theta}{Dt}\} \dot{\gamma} + \tfrac{1}{2} \theta \frac{\bar{D}}{Dt} \dot{\gamma} - \tfrac{1}{2}(\theta + 2\beta)(\dot{\gamma} \cdot \dot{\gamma}) + \quad .. \quad (C\text{-}1)$$

One must be prepared to sacrifice mathematical completeness for practical utility and in many instances, this recourse appears possible when viscoelastic effects are not of serious consequence. In simple shear flow, a power law description of the viscous characteristics is adequate for polymer solutions.

CHAPTER III

TUBE FLOW OF NON-NEWTONIAN FLUIDS

A. Introduction

The mechanical behavior of many real fluids, particularly those of low mol. wt. has been described by the theory of Navier-Stokes fluids over a wide range of circumstances. This theory is based upon the following equations:

$$\overleftrightarrow{\tau} = - p \overleftrightarrow{I} + 2\eta_o \overleftrightarrow{\Delta} \qquad \text{..... (A-1)}$$

$$\text{Trace } \overleftrightarrow{\Delta} = 0 \qquad \text{..... (A-2)}$$

where Δ is the rate of strain tensor, τ is the stress tensor, p is the isotropic pressure and η_o is the viscosity. For Navier-Stokes fluids, such as water, equations (A-1) and (A-2) predict that the volumetric flow rate will be proportional to the driving force and to the fourth power of the radius R of the pipe in steady Poiseuille flow. This simple relation does not hold for solutions of high polymers in simple shear flow. For polymer solutions, the viscosity is a function of shear rate. Many rheological models, discussed in Chapter II, have been proposed to approximate the flow behavior of the non-Newtonian fluids.

B. Flow Through Tubes

For steady, laminar, isothermal flow through tubes, expressions for flow rate and velocity distribution as functions

of pressure drop may be derived by substituting the appropriate constitutive equations, relating shear stress and shear rate, in general equations of motion and continuity. In the tube flow of solutions of high polymeric materials, however, the wall may introduce a preferred direction. This anomalous surface effect has been treated mathematically by Schofield and Scott Blair (47) and also by Oldroyd (39). They have outlined procedures to detect this effect near the solid boundary. Their methods were used successfully by Toms (51, 52) for his data on solutions of polymethyl methacrylate both in the laminar as well as turbulent flow. The mathematical expression developed by Oldroyd (16, 39) takes the form:

$$\frac{8\langle U\rangle}{D} = \frac{8\ U_w(\tau_w)}{D} + \frac{4}{\tau_w^3}\int_0^{\tau_w} \tau^2 f(\tau)\,d\tau \quad \ldots\ldots\ldots \quad (B\text{-}1)$$

The effective slip velocity, U_w, accounting for the anomalous flow behavior, has been found to be a function of shear stress at the wall. Equation (B-1) can be further written as

$$\frac{8\langle U\rangle}{D\ \tau_w} = \frac{8\ U_w(\tau_w)}{D\ \tau_w} + \frac{4}{\tau_w^4}\int_0^{\tau_w} \tau^2 f(\tau)\,d\tau \quad \ldots\ldots\ldots \quad (B\text{-}2)$$

$$\text{or} \quad {}^1/_{\eta'} = \frac{8}{D}\,\xi(\tau_w) + \frac{4}{\tau_w^4}\int_0^{\tau_w} \tau^2 f(\tau)\,d\tau \quad \ldots\ldots\ldots \quad (B\text{-}3)$$

Here ${}^1/_{\eta'}$ is called the apparent fluidity and $\xi(\tau_w)$ is called

the effective velocity of slip per unit shear stress at the wall. This analysis for tube flow has been extended to the case of flow between rotating coaxial cylinders by Oldroyd (16). Morrison and Harper (37) experimentally observed the wall effect in such flow for suspensions of fibrous particles. This analysis has been extended further by Kozicki et al (27) for the prediction of the flow rate and maximum velocity versus pressure drop relationships in the isothermal, steady, uniform, laminar flow of incompressible time-independent non-Newtonian fluids in complex-shaped flow channels. Jastrzebski (25) found that for his data on concentrated suspensions of kaolinite PD-10, the Oldroyd method did not give satisfactory results. It was found that the slip coefficient was not only a function of the shear stress but also varied inversely with the tube radius. This dependence on tube radius enabled satisfactory correlation of the data.

For the flow of aqueous polymer solutions in the intermediate and high shear rate range, another parameter, the critical shear stress, has been found to contribute to the peculiar separation observed in the flow curves. In the present analysis, a new slip coefficient is defined as follows:

$$\alpha(\tau_w, D) = \frac{U_w}{\tau_w - \tau_c(D)} \qquad \text{..... (B-4)}$$

with

$$\alpha(\tau_w, D) = \frac{\alpha'(\tau_w)}{D} \qquad \text{..... (B-5)}$$

where the critical shear stress τ_c is assumed to be some function of the tube diameter. The effective slip velocity thus can be written as:

$$U_w = \frac{\alpha'(\tau_w)}{D} \{\tau_w - \tau_c(D)\} \quad \ldots\ldots\ldots\ldots\ldots \quad (B\text{-}6)$$

Substituting this value of U_w in the equation (B-1), one obtains :

$$\frac{8\langle U\rangle}{D} = \frac{8\alpha'(\tau_w)}{D^2}\{\tau_w - \tau_c(D)\} + \frac{4}{\tau_w^3}\int_0^{\tau_w} \tau^2 f(\tau)d\tau \quad \ldots \quad (B\text{-}7)$$

Now, the slip coefficient α' can be obtained as the slope of the plot of $\frac{8\langle U\rangle}{D}$ versus $\frac{8}{D^2}\{\tau_w - \tau_c(D)\}$. This slip coefficient is then used to calculate the effective slip velocity which manifests the physical phenomenon taking place.

The polymer molecules are adsorbed on the tube wall at multiple points of attachment. Due to this adsorption, the effective tube diameter will be less and hence there will be decreased flow rate. This could be corrected by calculating the effective slip velocity from equation (B-6). Hence the true shear rate can be obtained after making this correction. This phenomena has been investigated experimentally and theoretically by many other workers. Luce and Robertson (31) studied the adsorption of polyvinyl acetate from solution by water-swollen bleached sulfite pulps. Koral, Ullman and Eirich (26) also investigated the adsorption of polyvinyl acetate by metallic powders. The adsorption phenomenon has

been similarly studied by Hobden and Jellinek (24), Frish, Hellman and Lundberg (19) and Yurzhenko and Maleyev (56). Sadowski (46) also observed this phenomenon in his packed bed experiments on Natrosol solutions. Many other workers have studied the phenomena theoretically by a statistical mechanical approach (46).

Polymer adsorption seems to be prominent in the lower shear rate region. As the shear stress is increased, the polymer molecules uncoil. This has been described as a central feature of polymer molecules by Merrill (1). Hence under shear stress, the molecules are distorted into increasingly elongated ellipsoids. These molecules will then tend to align in the direction of flow near the solid boundary. The molecular configuration also changes. This gradual change in structure to rod-like particles results in a less viscous layer near the solid boundary. As a result, the flow rate increases. Again, the correction has to be made to obtain the true shear rate. This separation phenomenon results in a positive effective slip velocity. The true shear rate, $8(\langle U \rangle - U_w)/D$, can be obtained after calculating the effective slip velocity. In summary, the proposed model should explain polymer adsorption and then the transition to the separation phenomenon observed in tubes of different diameters under varying shear stress.

C. Prediction of Transition from Laminar to Turbulent Flow

The mathematical model, discussed in the previous section,

could be used to describe the laminar flow of aqueous polymer solutions. Therefore, it is necessary to ensure that the flow condition is laminar. The correlation of the laminar, transition and turbulent flow regions for the flow of non-Newtonian fluids was given by Metzner and Reed (35). They defined a generalized Reynolds number and based on this a friction factor. The correlation of the data on the flow of non-Newtonian fluids in pipes was made on the conventional friction factor-Reynolds number plot. In their analysis, it was assumed that there was no slip at the wall. It was, however, necessary to incorporate the slip because of the increased evidence of its occurrence in the tube flow. Kozicki et al (28) redefined the Reynolds number-friction factor relationships accounting for the anomalous wall effects. As a result of this, the point of transition from laminar to turbulent flow of a fluid exhibiting anomalous behavior in laminar flow will be different from one which exhibits no anomalous effects. Meter (34) has presented a correlation scheme for polymers and polymer solutions to predict the point of transition into turbulent flow. His analysis uses the Ellis fluid model and does not take into account the anomalous flow behavior. Subsequently, Kozicki and Tiu (29) applied the Ryan-Johnson stability theory to predict the point of transition for anomalous flow. The expressions for the critical values of the friction factor, f_c, and the Reynolds number Re_c, are given by the following relationships:

$$f_c = \frac{1}{404}\left\{\frac{3n+1}{n+1}(1-\lambda_c)^{\frac{n+1}{n}} + \frac{U_w}{\langle U\rangle - U_w}\right\}\frac{3n+1}{n}(\lambda_c)^{1/n} \quad \ldots\ldots (C\text{-}1)$$

$$\text{and} \quad \lambda_c = \left(\frac{1}{n+2}\right)^{\frac{n}{n+1}}\left\{1+\frac{n+1}{3n+1}\frac{U_w}{\langle U\rangle - U_w}\right\}^{\frac{n}{n+1}} \quad \ldots\ldots (C\text{-}2)$$

$$Re_c = {}^{16}/_{f_c} \quad \ldots\ldots (C\text{-}3)$$

$$Re = \frac{D^{n'}(\langle U\rangle - U_w)^{2-n'}\rho}{8^{n'-1}K'} \quad \ldots\ldots (C\text{-}4)$$

For power law fluids, the critical friction factor is given as a function of the flow behavior index with the ratio of slip velocity to bulk velocity as the parameter. This method will be used to check these data.

D. Estimation of Anomalous Layer Thickness:

Polymer adsorption and separation play an important role in polymer behavior over a long range of shear rates and tube diameters. The anomalous layer thickness for these phenomena can be calculated based on Oldroyd's analysis. For tube flow, the velocity gradient in the anomalous layer within a radial distance δ from the solid boundary can be represented by:

$$\frac{du}{dy} = f(\tau) + g(\delta,\tau,y) \quad \ldots\ldots (D\text{-}1)$$

where $f(\tau)$ is the velocity gradient depending on the fluid model and $g(\delta,\tau,y)$ is a term accounting for the anomalous behavior in the vicinity of the wall. Integrating equation (D-1) within the limits 0 to y greater than δ, one obtains:

$$U = f(\tau_w)y + \int_0^{\delta} g(\delta,\tau_w,y)\,dy \quad \ldots\ldots\ldots\ldots\ldots\ldots \quad (D\text{-}2)$$

$$\text{or} \quad U - U_w(\delta,\tau_w) = f(\tau_w)y \quad \ldots\ldots\ldots\ldots\ldots\ldots\ldots \quad (D\text{-}3)$$

$$\text{where } U_w(\delta,\tau_w) = \int_0^{\delta} g(\delta,\tau_w,y)\,dy$$

From equation (D-3), it is clear that when $y=0$, $U = U_w(\delta,\tau_w)$. This is referred to as the effective velocity of slip at the wall. When $g(\delta,\tau_w,y)$ is positive, the anomalous layer is less viscous than the fluid in the main stream giving rise to a positive effective velocity of slip. On the other hand when $g(\delta,\tau_w,y)$ is negative, the presence of the wall gives rise to a more viscous layer than the main stream, resulting in negative effective velocity at the wall. In the present study, both kinds of phenomena are observed and it is seen that the transition also takes place.

An estimate of the thickness of the anomalous layer can be easily done. When the layer adjacent to the wall is pure solvent, the so called "separation phenomenon" (2), the velocity gradient in the anomalous layer is given by τ_w/μ_s. Thus equation (D-1) can be written as:

$$U_w(\delta,\tau_w) = \delta\{\frac{\tau_w}{\mu_s} - f(\tau_w)\} \quad \ldots\ldots\ldots\ldots\ldots \quad (D\text{-}4)$$

This can be solved for δ if the effective slip velocity and the constitutive equations are known. Similarly, when the

effective velocity at the tube wall is negative, accounting for polymer adsorption, the velocity gradient can be assumed to be zero in the vicinity of the wall and the layer thickness can be computed from the relation:

$$U_w(\delta,\tau_w) = -\delta\, f(\tau_w) \qquad \text{..... (D-5)}$$

The shear rate $f(\tau_w)$, required to calculate the anomalous layer thickness, is found from the following relationship (28):

$$(-\frac{du}{dr})_w = f(\tau_w) = \frac{1+3n'}{4n'}\{\frac{8(<U>-U_w)}{D}\} \qquad \text{..... (D-6)}$$

E. Determination of Flow Curve:

Rabinowitsch and Mooney (36, 42) developed an expression for the rate of shear of a fluid which is entirely independent of the fluid properties, provided thixotropy and rheopexy are eliminated. Their final expression can be written in the form:

$$(-\frac{du}{dr})_w = \frac{3}{4}(\frac{8<U>}{D}) + \frac{1}{4}\frac{D\Delta P}{4L}\cdot\frac{d(\frac{8<U>}{D})}{d(\frac{D\Delta P}{4L})} \qquad \text{..... (E-1)}$$

In this analysis by Rabinowitsch and Mooney, the effect of anomalous flow behavior was not taken into account. Kozicki et al (27) modified the equation (E-1) which now includes the effective slip velocity and also the geometric parameters:

$$\left(-\frac{\partial u}{\partial \bar{n}}\right) = f(\tau_w) = a\,\tau_w \frac{d\left\{\frac{2(<U>-U_w)}{r_H}\right\}}{d\,\tau_w} + b\left\{\frac{2(<U>-U_w)}{r_H}\right\} \cdots \quad (E\text{-}2)$$

Here the geometric parameters take the values, $a=\frac{1}{4}$, $b=\frac{3}{4}$ for circular cross section. It is evident from equation (E-2) that $f(\tau_w)$ is a function of the shear stress at the wall and depends upon the fluid model. The equation (E-1) was further rearranged by Metzner and Reed (35) to give:

$$\left(-\frac{du}{dr}\right)_w = \frac{3}{4}\left(\frac{8<U>}{D}\right) + \frac{1}{4}\left(\frac{8<U>}{D}\right)\frac{d\left(\frac{8<U>}{D}\right)\cdot\left(\frac{8<U>}{D}\right)}{d\left(\frac{D\Delta P}{4L}\right)/\left(\frac{D\Delta P}{4L}\right)} \quad \cdots\cdot \quad (E\text{-}3)$$

$$= \frac{3}{4}\left(\frac{8<U>}{D}\right) + \frac{1}{4}\left(\frac{8<U>}{D}\right)\frac{d\ln\left(\frac{8<U>}{D}\right)}{d\ln\left(\frac{D\Delta P}{4L}\right)} \quad \cdots\cdots\cdot \quad (E\text{-}4)$$

The following expression analogous to equation (E-4), incorporating the effective slip velocity can be written as

$$\left(-\frac{du}{dr}\right)_w = \frac{3}{4}\left\{\frac{2(<U>-U_w)}{r_H}\right\} + \frac{1}{4}\left\{\frac{2(<U>-U_w)}{r_H}\right\}\frac{d\ln\frac{2(<U>-U_w)}{r_H}}{d\ln\,\tau_w} \cdots \quad (E\text{-}5)$$

If the derivative in equation (E-5) is denoted by $1/n^*$, one obtains:

$$\left(-\frac{du}{dr}\right)_w = \frac{3n^*+1}{4n^*}\cdot\left\{\frac{2(<U>-U_w)}{r_H}\right\} \cdots\cdots\cdots\cdots \quad (E\text{-}6)$$

$$\text{where } n^* = \frac{d\{\ln \tau_w\}}{d\{\ln \frac{2(<U>-U_w)}{r_H}\}} \quad \ldots\ldots\ldots\ldots\ldots\ldots \quad (E\text{-}7)$$

The equation (E-7) can be written in the form:

$$\frac{D\Delta P}{4L} = \tau_w = K^* \left\{\frac{2(<U>-U_w)}{r_H}\right\}^{n^*} \quad \ldots\ldots\ldots\ldots \quad (E\text{-}7')$$

When the effective velocity of slip is zero, this expression yields the expression given by Metzner and Reed (35):

$$\tau_w = K' \left(\frac{8<U>}{D}\right)^{n'} \quad \ldots\ldots\ldots\ldots\ldots\ldots\ldots \quad (E\text{-}8)$$

This expression is superficially similar to the power law relation which for pipe flow may be written:

$$\dot{\tau} = K \left(\frac{du}{dr}\right)^{n} \quad \ldots\ldots\ldots\ldots\ldots\ldots\ldots \quad (E\text{-}9)$$

K* and n* are closely related to K and n. For power law fluids, K* and K' are the same and are related to K by

$$K^* = K' = K \left(\frac{3n+1}{4n}\right)^{n} \quad \ldots\ldots\ldots\ldots\ldots \quad (E\text{-}10)$$

K* is a measure of the consistency of the material and is known as the consistency index and n* is that physical property of the fluid which characterizes its degree of non-Newtonian behavior and is known as flow behavior index. If

the logarithmic plot of $\frac{D\Delta P}{4L}$ versus $\frac{8\langle U\rangle}{D}$ or $\frac{8(\langle U\rangle - U_w)}{D}$ is a straight line, n becomes equal to n' or n*. Equation (E-7)' is of practical importance. It can be used in pipe line design provided K* and n* values applicable to the shear stress under consideration are used.

The raw experimental viscometer data consist of flow rate versus applied pressure. These can be converted into shear stress and shear rate data. Before doing so, some corrections must be made to obtain the true pressure gradient. The corrections are for the following effects (49).

(1) Head of fluid above the tube exit.

(2) Kinetic energy effects.

(3) Tube entrance effects.

A total mechanical energy balance yields the expression for the frictional pressure drop across the capillary tube in fully developed flow

$$-\frac{dP}{dx} = \frac{Pgas-Pa}{L} + \frac{(L + L')}{L}\ \rho\frac{g}{g_c} - \frac{\rho\langle V\rangle^2}{g_c L}\left(\frac{1}{2\alpha} + \frac{K_c}{2}\right) \quad \ldots \text{(E-11)}$$

For Newtonian fluids in fully developed laminar flow, α has the value of $\frac{1}{2}$. The cut end of the capillary tube is usually trimmed to result in a slighted rounded entrance. For such cases, Foust et al (18) quote a value of 0.23 for K_c for Newtonian materials. Hence, one obtains the final expression for Newtonian fluids

$$-\frac{dP}{dx} = \frac{P_{gas} - Pa}{L} + \frac{(L + L')}{L}\rho\frac{g}{g_c} - 1.12\frac{\rho\langle V\rangle^2}{L g_c} \quad \ldots\ldots\ldots \text{(E-12)}$$

For non-Newtonian fluids, uncertainties exist regarding these corrections. In the present experimental work, L/D has been taken very large so that the entrance correction is negligible. Bagley (4) has suggested the empirical method for eliminating entrance effects. However, the procedure requires the assumption of a zero slip velocity at the tube wall. Equation (E-12) is used to obtain the true pressure gradient and equivalent shear stress.

CHAPTER IV

FLUIDS AND THEIR PREPARATION

Most high molecular wt. polymers in aqueous solution are pseudoplastic or shear thinning non-Newtonian fluids, characterized by absence of yield value. These polymers exhibit many interesting phenomena because of diversified polymer behavior in solution.

When polymer solutions are viscometrically examined at low shear rate and high dilution, each dissolved macromolecule (which occupies an enormous volume relative to its unsolvated size) approaches the ideal state of complete hydrodynamic independence of other macromolecules and negligible perturbation of its configuration in the solvent under zero flow. But in polymer solutions of industrial and engineering interest, the shear rate and level of concentration are large enough to preclude hydrodynamic independence and unperturbed configuration. Several polymer solutions have been examined and interesting facts have been presented by Merrill (32).

In the present investigation, Natrosol solutions were studied at high shear rates. Natrosol has been described as a linear polymer with only a slight degree of chain branching but with a more restricted rotation about the connecting bonds (46). Natrosol is a nonionic water soluble polymer derived from cellulose. Like Na-CMC, it is a cellu-

lose ether, but it differs in being nonionic and its solutions are unaffected by cations. Natrosol has been used as a thickener, protective colloid, binder, stabilizer and suspending agent in a variety of industrial applications, including pharmaceuticals, textiles, paper, adhesives, decorative, and protective coatings, emulsion polymerisation, ceramics etc. Natrosol is produced in three degrees of substitution, designated as Natrosol 180, Natrosol 250, Natrosol 300. Natrosol 250 in two grades (G and HR) was used in the present experimental work. The possible molecular structure of Natrosol 250 is shown in the following diagram.

It is believed (21) that cellulose derivatives do not possess a spherical symmetry in solution but rather a slightly extended rod configuration due to the stiffness of the chain. There is no definite information about the molecular wt. of these polymers. According to Goring (21) the molecular wt. should be comparable to that of CMC which is in the range of 15×10^4 to 35×10^4. So, the high molecular wt. Natrosol solutions will extend the "degree of non-Newtonianess".

Natrosol solutions were prepared by dissolving the polymers in water. The procedure used was the one recommended by the manufacturer*. Natrosol was sifted slowly into the vortex of vigorously agitated water. The

*Hercules Powder Co.

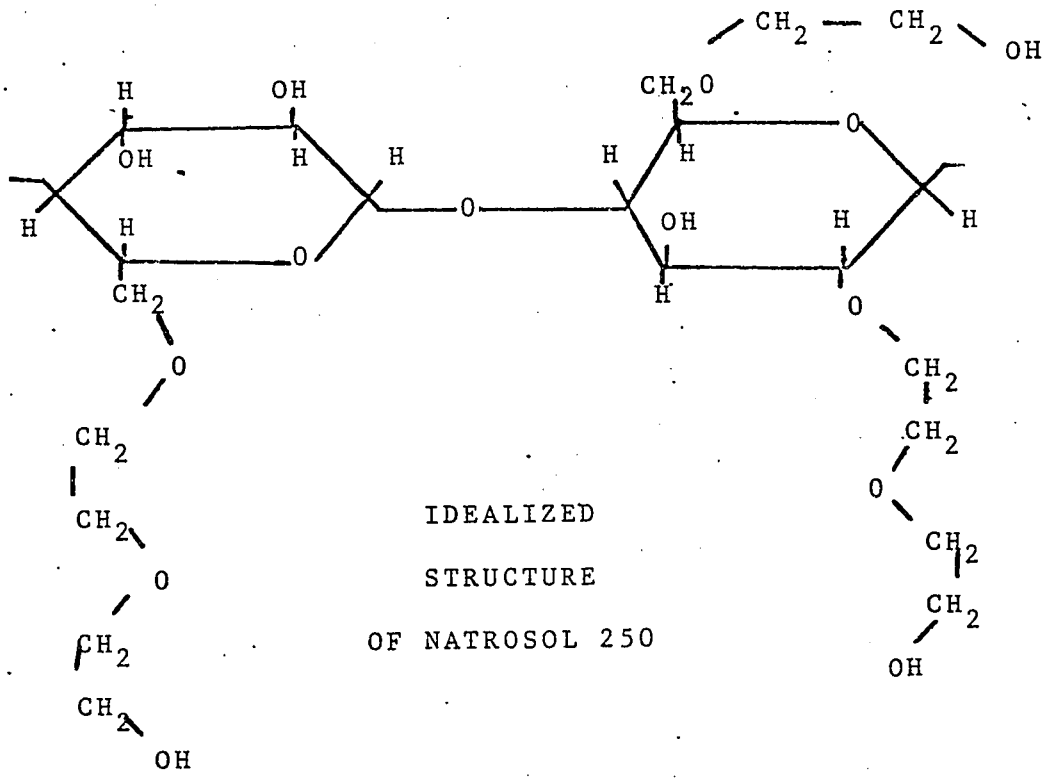

IDEALIZED

STRUCTURE

OF NATROSOL 250

rate of addition was kept low enough for the particles to separate in water without lump formation. The agitation was continued until all of the swollen particles were dissolved to yield a clear solution. The time required was usually about one hour to two hours. Four concentrations of Natrosol-250 G and HR each were prepared to study the flow behavior of the polymers in aqueous solution. The concentrations for Natrosol-250 G were 0.6%, 0.8%, 1.0% and 1.2% by weight and for Natrosol-250 HR 0.1%, 0.2%, 0.3% and 0.4% by wt.

CHAPTER V

VISCOMETRIC EXPERIMENTS

In order to carry out meaningful engineering calculations for non-Newtonian fluid systems, it is essential that the appropriate rheological properties be known. In Chapter III, a description of some of the parameters and equations suitable for representing the tube-flow of non-Newtonian fluids was given.

There are several types of viscometers (8), used for characterization of non-Newtonian fluids. The viscometers (49) used in the laboratory experimental work are:

(1) the Capillary Viscometer or Extrusion Rheometer.

(2) the Concentric Cylinder Rotary Viscometer.

(3) the Rotating Cylinder in an Infinite Medium.

(4) the Cone and Plate Type Rotary Viscometer.

The commercial versions of the viscometers have been described extensively by Van Wazer, et al (54).

A. Capillary Viscometer

This is a device by means of which the relationship between shear rate and shear stress is inferred indirectly from measurements of the pressure gradient and volumetric flow rate in a cylindrical tube of precisely known dimensions. The most common features of the Capillary Viscometer are:

(1) Fluid Reservoir

(2) Capillary Tube

(3) Means for applying a driving force on the fluid

(4) A thermoregulating device

It is a common practice to construct this viscometer in the laboratory (8, 48). In the present study, a laboratory designed viscometer was used in determination of the flow curves of aqueous polymer solutions. The viscometer consists of a reservoir, 7.30 cm. in diameter and about 35 cm. high. The material of construction was stainless steel pipe of thickness 0.78 cm. The lower portion was welded to a standard flange joint making it easy to take the equipment apart for cleaning. A hexagonal nut with internal bore was welded to the lower flange so that capillary tubes of different diameters and lengths can be fastened. Standard sleeves and male glands for Ermeto connections were used. The upper portion of the rheometer held connections necessary for introducing the gas and the fluid and a connection leading to a pressure gauge and for releasing the pressure. Tangential entrance of the gas prevented its mixing with the fluid and formation of gas bubbles.

An important advantage of the extrusion rheometer over other types of viscometric equipment lies in the fact that the liquid resides in the tube only for very short times. The continuous fluid replenishment reduces the accumulation of heat due to viscous energy dissipation in the fluid. In other types of viscometric equipment, all the energy must

be conducted out of the fluid sample to avoid errors due to non-isothermal flow conditions. Further, it has been shown by Toors (53) that in this kind of viscometer, the temp. rise due to possible viscous heat dissipation is negligible. For example, for a fluid having a viscosity of 1,000 cp at a shear rate of 10^4 sec.$^{-1}$ flowing through a 0.025" dia. tube with an L/D of 500, the maximum temp. rise anywhere in the fluid would be less than 1^o F. These flow conditions, requiring a pressure drop of about 3,000 psi. per ft. of tube length are obviously extreme so that the temp. rise may usually be neglected in solutions and slurries.

Several capillary tubes over a wide range of lengths and diameters were employed in the present study. Hypodermic needle tubings of type 304 austenitic chromium nickel stainless steel, supplied by Superior Tube, Norristown, Pa., were used. The range of lengths of the different dia. tubes varied from 17 cms. to 46 cms. The lengths were measured by a micrometer. The diameter range used in the present work was from 0.0578 cm. to 0.0184 cm. The deviations in diameter, provided by the manufacturer, were reported as -10.50% to +5.26%. Two Newtonian fluids, distilled water and ethylene glycol* (99.93% pure), were used to calibrate the tubes. Two sets of experimental data with different tubes were taken on each fluid. In the distilled

*Supplied by Fischer Scientific Co.

water calibration, the deviations obtained from the manufacturer's reported diameters ranged from +3.88% to -2.35%. With ethylene glycol, the deviations obtained were from +9.36% to +0.77%. Some of the tubes were also calibrated by Filled Microscope Probes Method. The deviation from the reported value found by this method was about the same as that for distilled water and ethylene glycol. All deviations were within the range given by the manufacturer. It was decided to use the calibrated diameters obtained with distilled water since they appeared to be most accurate. These are tabulated in the Appendix. Since the tubes were flexible because of the lengths used, they were enclosed by protective stainless steel tubes. These were welded near one end of the capillary tube. The L/D ratios employed were in the range of 400 to 1,100.

A schematic diagram of the experimental set up is shown in figure (1). The capillary tube is fastened to the base of the reservoir by a hand tightened cap. The major portion of the tube was kept inside the viscometer (8) to obtain uniform temp. throughout the capillary length. Water was circulated from a const. temp. bath through a reservoir holding the fluid and through a water jacket, surrounding the viscometer assembly. The const. temp. circulating system was obtained from Precision Scientific Co., Chicago, Ill. This was fitted with an adjustable Micro-Set Thermoregulator which gave a control sensitivity of $\pm$ 0.01^{o} C, over the

entire range.

The equipment was standardized with two Newtonian fluids, distilled water and ethylene glycol (99.93%) before taking runs on experimental fluids. The shear rate versus shear stress curve shown in the figure (2) indicates no wall effects for ethylene glycol and a slope of unity for the curve gives n = 1 for Newtonian fluid. The non-Newtonian fluids employed were solutions of Natrosol-250 G and Natrosol 250 HR in distilled water. Each polymer was studied at four different concentrations to cover a wide range of the flow behavior index. For each concentration, data were taken with tubes of different diameters and lengths. Reproducibility of the data was within 5.0%. Densities were determined by weighing known volumes of the solutions in a pycnometer. The volume rate of flow was obtained by weighing the liquid collected over a measured time interval. Pressure drop was measured by means of a USG test gauge with an accuracy of (a) 0.2% of scale range for first 20% of the range (b) 0.5% of indicated reading for remainder of the dial range in the pressure ranges employed (10-350 p sig).

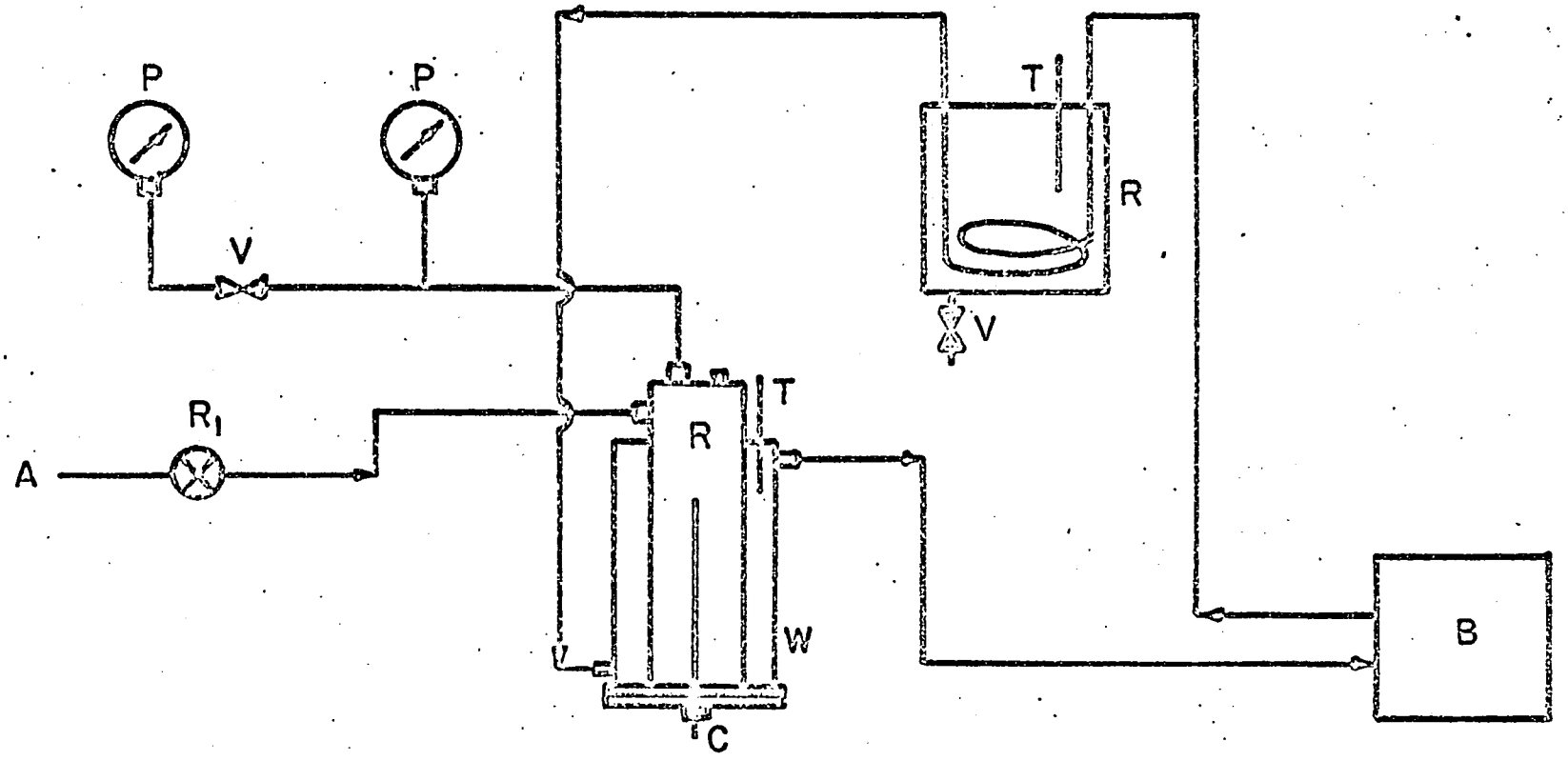

A - COMPRESSED AIR

B - CONST. TEMP. WATER BATH

C - CAPILLARY TUBE

P - PRESSURE GAUGES

R_1 - PRESSURE REGULATOR

R - FLUID RESERVOIRS

T - THERMOMETERS

V - VALVES

W - WATER JACKET

Figure 1. Schematic Diagram of the Experimental Set-Up

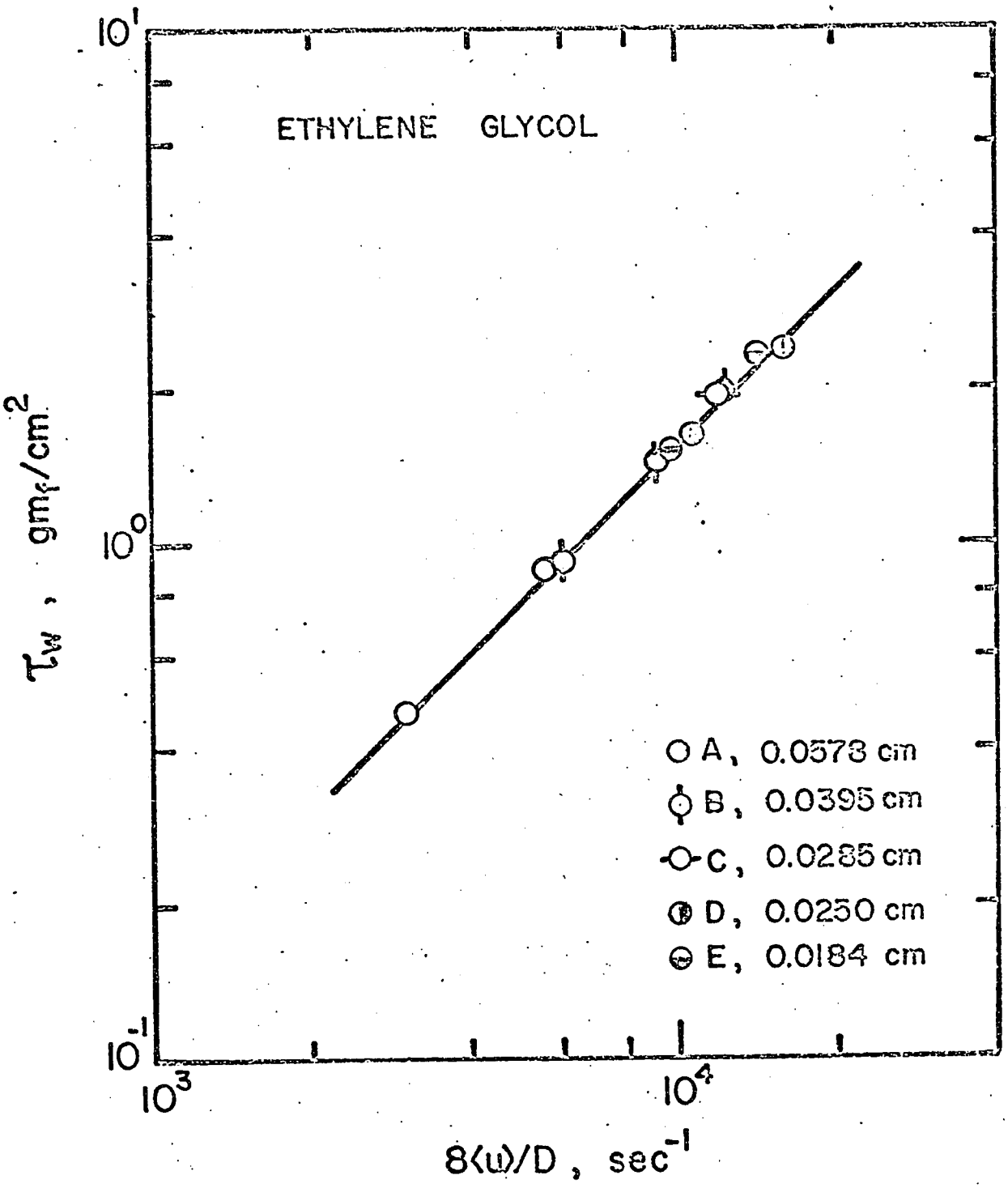

Figure 2.

Shear Stress versus Shear Rate Curve for Ethylene Glycol at 25°C for Different Tube Diameters

CHAPTER VI

RESULTS OF ANALYSIS

In the year 1949, Toms (52) successfully used the two methods (39, 47) of detecting wall effects in laminar flow of linear polymer solutions. Later, Jastrzebski(25) extended Oldroyd's method to the flow of concentrated suspensions. Presently, the anomalous flow behavior of polymer solutions was studied in intermediate and high shear stress regions. Four different concentrations of Natrosol-250 G and HR solutions were investigated. The experimental viscometric results are given in Appendix I.

The analysis of the data is based on the theoretical development given in Chapter III. Flow curves for 0.6%, 0.8%, 1.0% and 1.2% Natrosol-250 G are given in figures (3, 4, 5, 6) respectively. Except for 0.6% Natrosol-250 G solution, separate $8\langle U\rangle/D$ versus τ_w curve was obtained for each tube diameter suggesting the existence of anomalous surface effects. It is seen that the flow curves for these concentrations tend to intersect. This suggests the presence of a critical shear stress which marks the transition from a positive effective velocity to a negative effective velocity at the wall. Physically, the critical shear stress determines the behavior of polymer macromolecules in the vicinity of the tube wall. When the applied shear stress is smaller than the critical shear stress, polymer adsorption

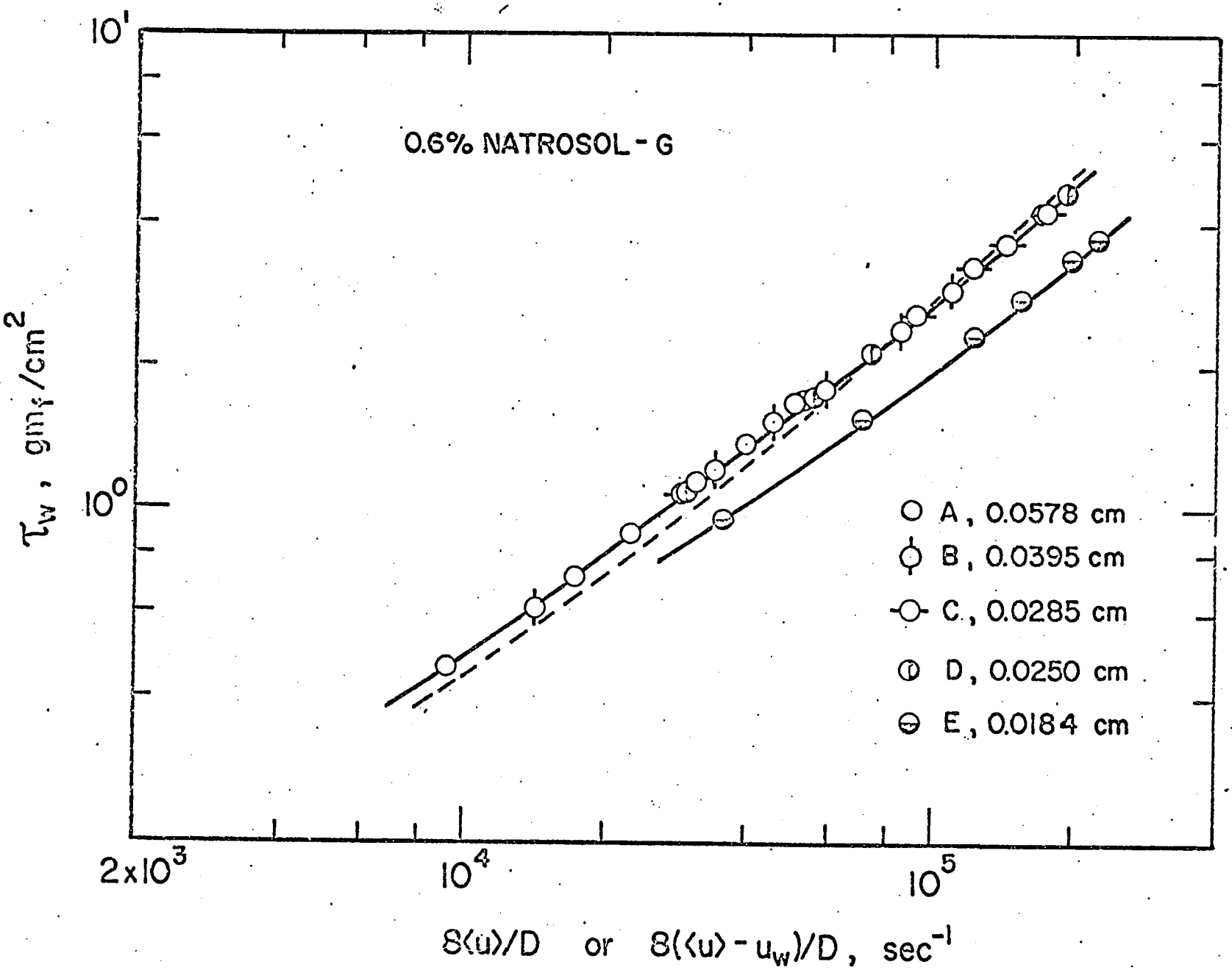

Figure 3. $8\langle U\rangle/D$ or $8(\langle U\rangle - U_w)/D$ versus τ_w for 0.6% Natrosol-250 G Solution at 25°C.

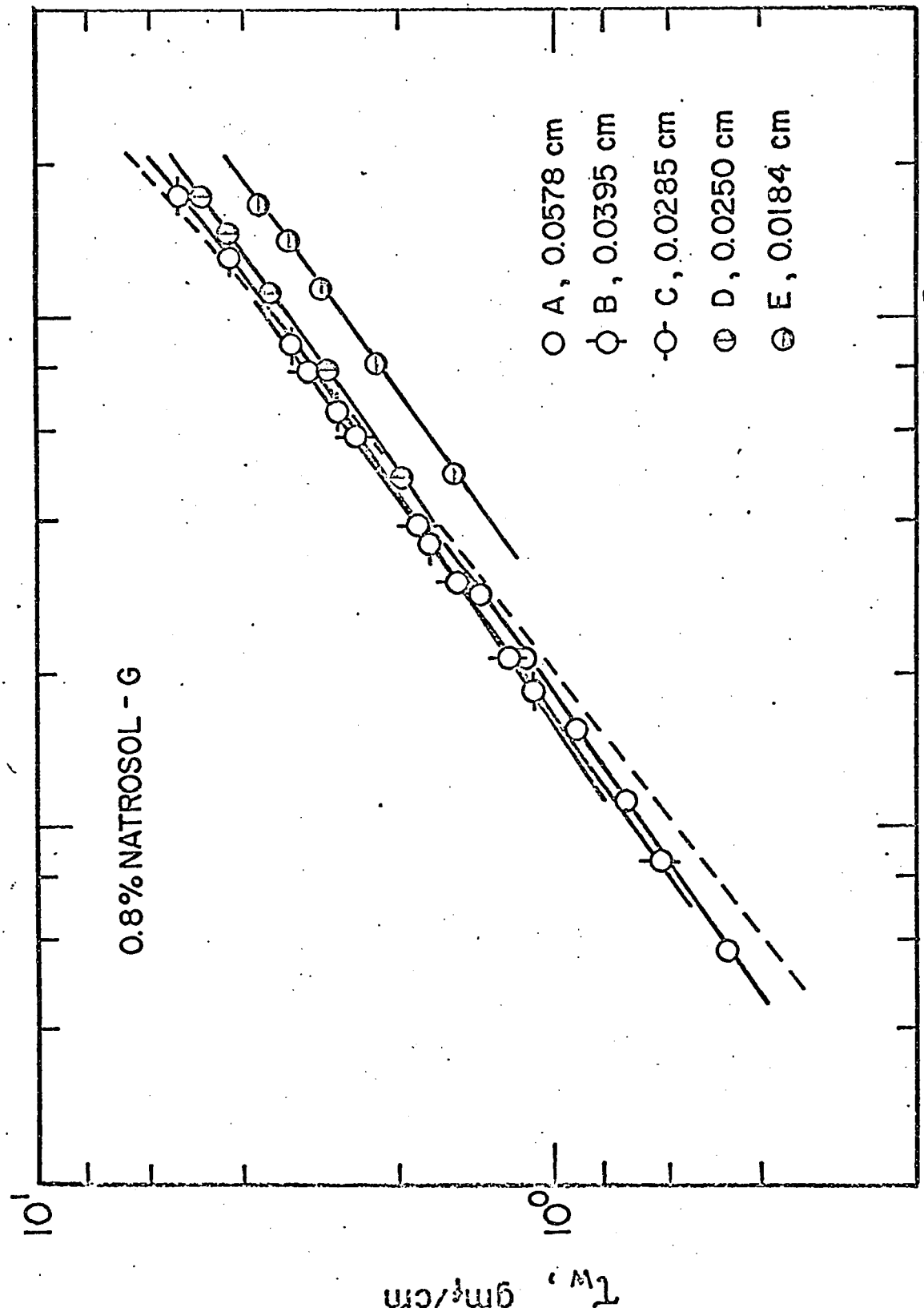

Figure 4. $8\langle U\rangle/D$ or $8(\langle U\rangle - U_w)/D$ versus τ_w for 0.8% Natrosol-250 G Solution at 25°C

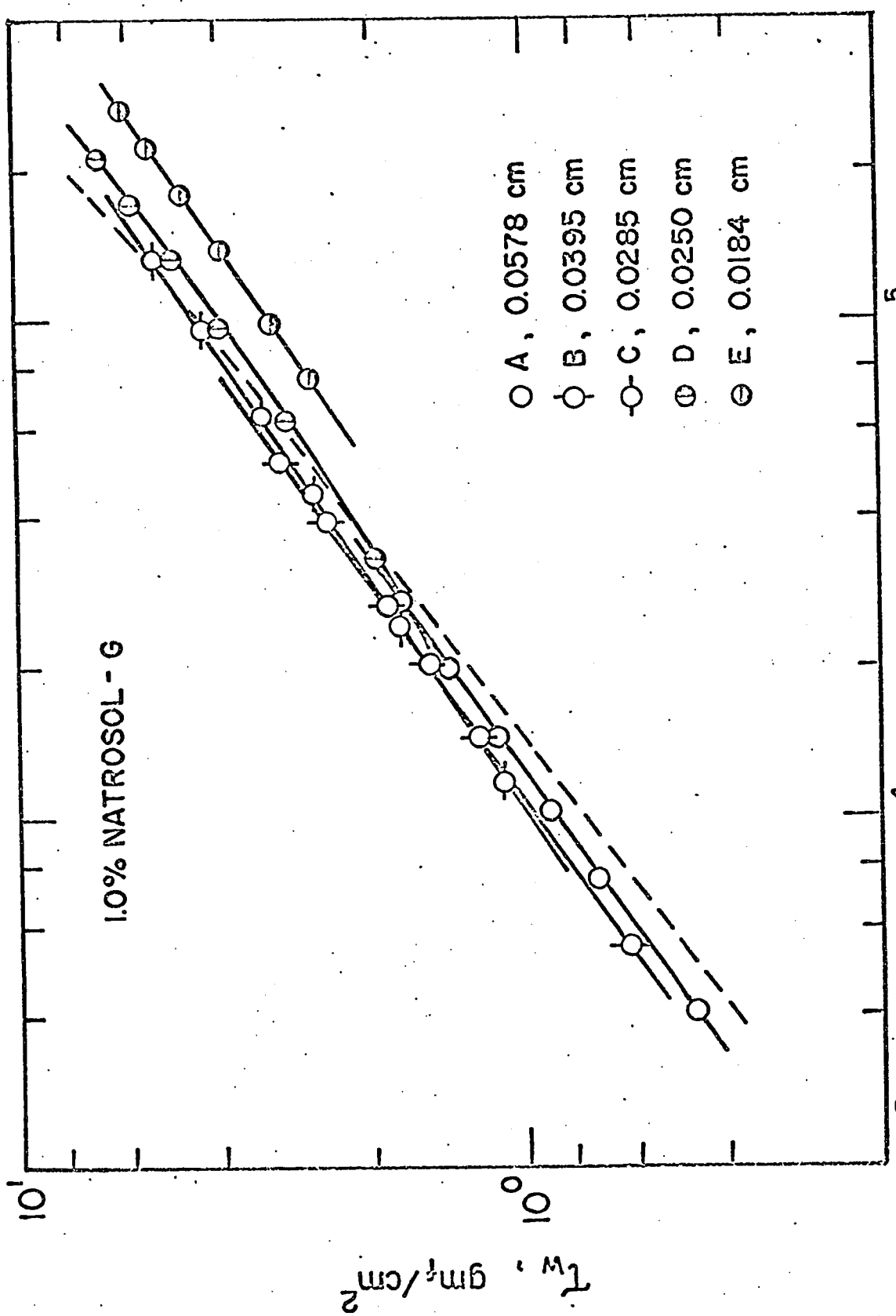

Figure 5. $8\langle U\rangle/D$ or $8(\langle U\rangle - U_w)/D$ versus τ_w for 1.0% Natrosol-250 G Solution at 25°C

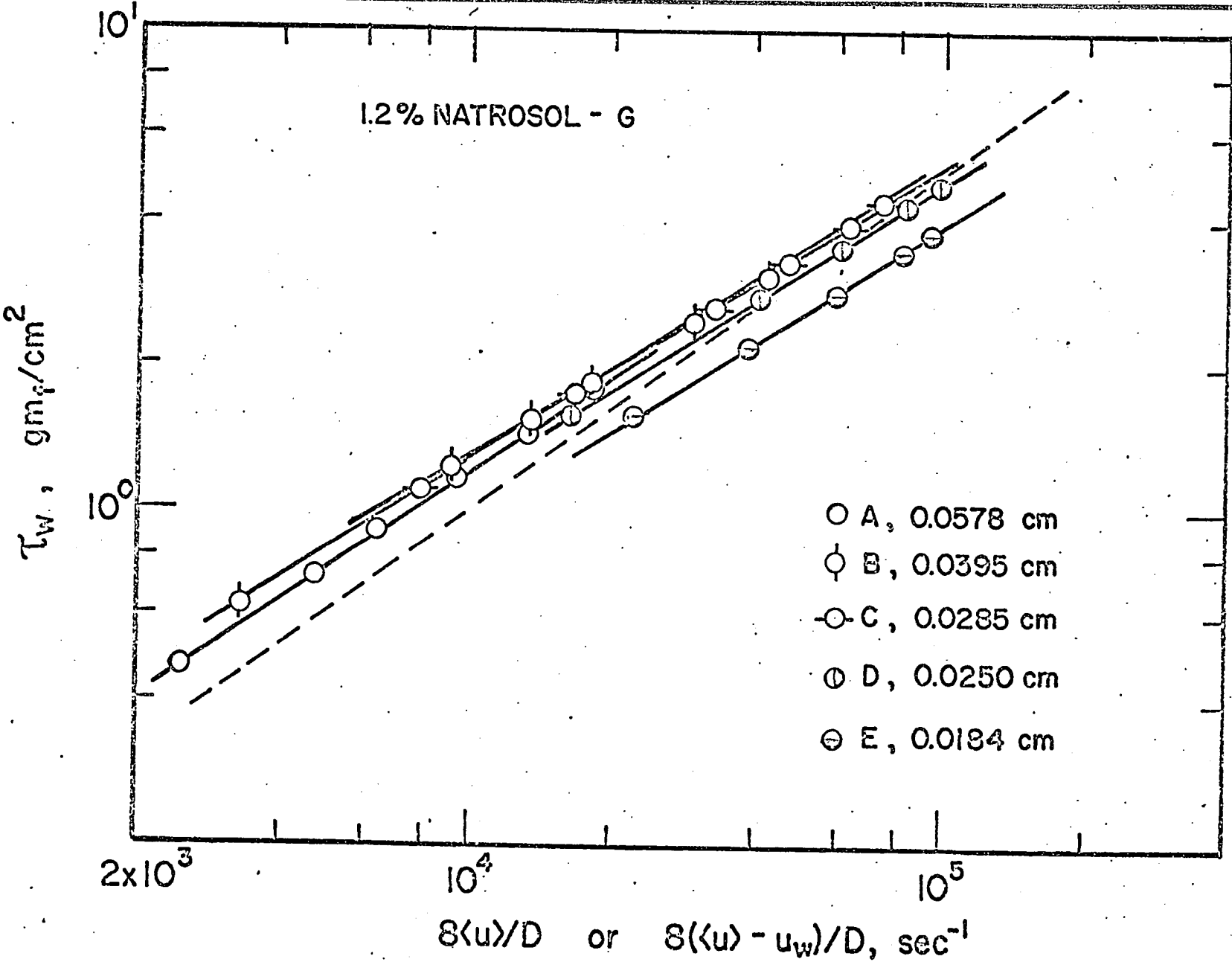

Figure 6. $8\langle U\rangle/D$ or $8(\langle U\rangle - U_w)/D$ versus τ_w for 1.2% Natrosol-250 G Solution at 25°C

or gel formation is postulated to occur. If the applied shear stress is greater than the critical shear stress, a separation phenomenon or a possible polymer alignment occurs. A careful analysis indicates that τ_c is some function of the tube diameter for a particular concentration. The trend of the curves on shear stress-shear rate plot suggests that the critical shear stress decreases with a decrease in tube diameter. A trial and error procedure gave a series of values for τ_c for different diameters which fit the data to a single flow curve. The final values of τ_c are given in Table (1). Figure (7) shows the variation of τ_c with concentration, with the tube diameter as parameter.

The broken lines in figures (3, 4, 5, 6) indicate the final curves of $8(<U>-U_w)/D$ versus τ_w determined for the various concentrations. When the values of the effective slip velocities are calculated, the corrections are applied to the experimental points. The calculated values for the effective velocity of slip are given in Tables (3, 4, 5, 6, 7) for various concentrations and tube diameters. In figure (11), the data points for different tube diameters merge into a single curve characteristic of Natrosol concentration. These curves correspond to the broken lines in figures (4, 5, 6).

In figure (3), the separation between the data points obtained with different tube diameters for 0.6% Natrosol-250 G solution is not completely evident except for capillary tube E. However, the possibility of surface effects cannot

TABLE I

Values of Critical Shear Stress

Capillary	τ_c, gm_f/cm^2			
	0.6% Natrosol-G †	0.8% Natrosol-G	1.0% Natrosol-G	1.2% Natrosol-G
A	5.50	6.80	8.00	9.00
B	3.90	4.80	6.20	7.30
C	2.55	3.40	4.00	5.00
D	1.65	2.10	2.50	3.00
E	0.10	0.30	0.40	0.60

† Values of τ_c for 0.6% Natrosol-G were obtained by extrapolation from higher concentrations (Fig. 7).

TABLE 2

Highest Reynolds Numbers and Their Corresponding Critical Points For Each Solution and Tube Diameter

I 0.8% NATROSOL-250 G

TUBE	DIAMETER, cm	τ_w, gm_f/cm^2	<U>, cm/sec	U_w, cm/sec	Re	Re_c
A	0.0578	1.7360	279.50	-33.50	486	2420
B	0.0395	2.9750	388.00	-30.20	466	2340
C	0.0285	5.3220	620.00	79.00	468	1940
D	0.0250	4.7960	542.50	113.80	318	1780
E	0.0184	3.7320	386.00	153.10	126	1385

II 1.0% NATROSOL-250 G

TUBE	DIAMETER, cm	τ_w, gm_f/cm^2	<U>, cm/sec	U_w, cm/sec	Re	Re_c
A	0.0578	1.7656	191.50	-30.20	226	2535
B	0.0395	3.0180	256.20	-38.60	247	2450
C	0.0285	5.3790	476.00	41.70	290	1975
D	0.0250	6.7830	666.00	186.00	279	1610
E	0.0184	6.1800	618.00	311.00	131	1135

TABLE 2I (cont'd)

III NATROSOL-250 G (1.2%)

TUBE	DIAMETER, cm	τ_w, gm_f/cm^2	<U>, cm/sec	U_w, cm/sec	Re	Re_c
A	0.0578	1.7780	132.50	-22.90	116	2600
B	0.0395	3.0290	208.00	-33.80	158	2580
C	0.0285	4.3450	263.00	-10.30	148	2342
D	0.0250	4.7240	302.00	33.50	130	2040
E	0.0184	3.7580	213.00	66.40	48.6	1595

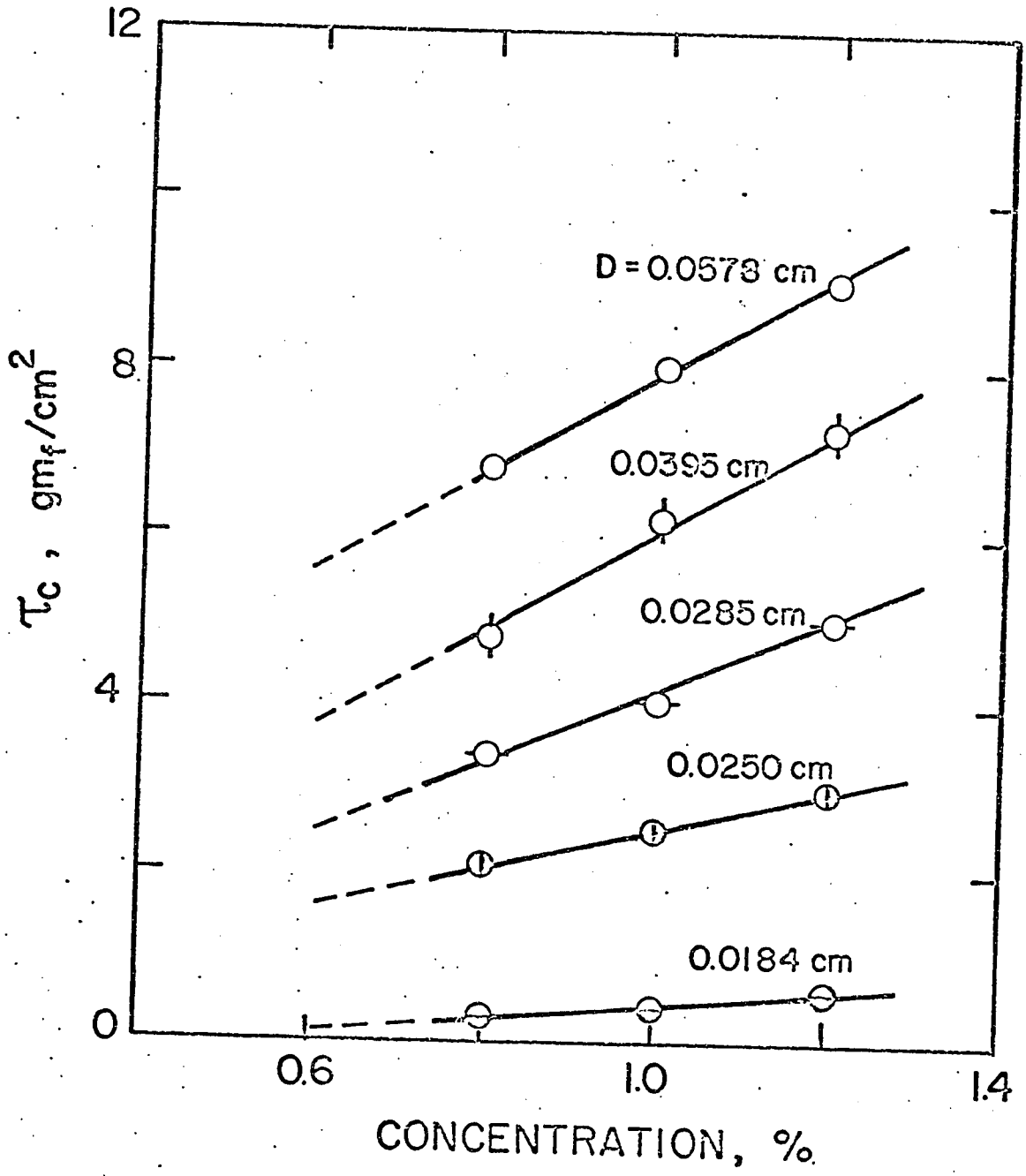

Figure 7. Critical Shear Stress versus Concentration of Natrosol-250 G Solutions at Different Tube Diameters

be ruled out. It is probable that the magnitude of the slip velocities involved for this concentration is so small that the separation of the individual curves was not discernible. One expects that as the concentration decreases, the behavior approaches that of the solvent. An alignment of the molecules along the tube axis seems to be prominent in the tube E, which is responsible for the separation in curve obtained. One can obtain the final shear rate versus shear stress curve by obtaining the critical shear stress values by extrapolation from the higher concentration shown in figure (7). The broken line in figure (3) represents the final flow curve based on τ_c values obtained by extrapolation of the data in figure (7) to lower concentration.

A slight curvature in the shear rate-shear stress curves depicting the fluid behavior is evident. Table (8) gives the parameters representing the viscous flow behavior of four Natrosol-250 G solutions in various shear stress ranges. The flow behavior index n' varies from about 0.70 to 0.96. No definite trend could be established for the variation of the flow behavior index with concentration. Generally speaking, as the concentration increases, the non-Newtonian behavior is more pronounced. The variation in the value of n' over the shear stress range is typical for pseudoplastic fluids. The flow behavior index approaches unity, indicating that the Upper Newtonian regime will be obtained at high shear stress. It was, however, not possible to obtain the

TABLE 3

Results for Capillary A

SOLUTION: 0.8% NATROSOL-250 G

τ_w, gm_f/cm^2	U_w, cm/sec	$\frac{8(<U>-U_w)}{D} \times 10^{-4}$, sec^{-1}	$\delta X 10^4$, cm
0.4630	-11.18	0.7220	14.38
0.7248	-16.80	1.3490	11.57
0.8967	-20.15	1.8500	10.11
1.1538	-24.80	2.4870	9.32
1.4083	-28.85	3.2450	8.40
1.7358	-33.50	4.3330	7.32

SOLUTION: 1.0% NATROSOL-250 G

τ_w, gm_f/cm^2	U_w, cm/sec	$\frac{8(<U>-U_w)}{D} \times 10^{-4}$, sec^{-1}	$\delta \times 10^4$, cm
.4636	- 9.77	0.5460	16.52
.7274	-14.50	0.9510	14.07
.9021	-17.40	1.2770	12.58
1.1631	-21.90	1.7800	11.36
1.4211	-25.60	2.3700	9.97
1.7656	-30.1903	3.1670	8.800

TABLE 3 (cont'd)

SOLUTION: 1.2% NATROSOL-250 G

τ_w, gm_f/cm^2	U_w, cm/sec	$\frac{8(<U>-U_w)}{D} \times 10^{-4}$, sec^{-1}	$\delta \times 10^4$, cm
.4641	- 7.06	0.3470	18.40
0.7287	-10.74	0.6180	15.74
0.9046	-13.05	0.8160	14.48
1.1681	-16.30	1.1650	12.67
1.4300	-19.29	1.5950	10.95
1.7777	-22.88	2.1520	9.62

TABLE 4

Results for Capillary B

SOLUTION: 0.8% NATROSOL-250 G

τ_w, gm_f/cm^2	U_w, cm/sec	$\frac{8(<U>-U_w)}{D} \times 10^{-4}$, sec^{-1}	$\delta \times 10^4$, cm
.6212	-14.50	1.1570	11.65
1.2237	-24.40	2.6550	8.58
1.5217	-27.80	3.5740	7.36
1.8177	-30.10	4.5030	6.34
2.4017	-32.10	6.4960	4.70
2.9752	-30.20	8.4640	3.41

SOLUTION: 1.0% NATROSOL-250 G

τ_w, gm_f/cm^2	U_w, cm/sec	$\frac{8(<U>-U_w)}{D} \times 10^{-4}$, sec^{-1}	$\delta \times 10^4$, cm
.6218	-14.00	0.8350	15.48
1.2269	-24.55	1.9510	11.62
1.5277	-28.60	2.6240	10.06
1.8276	-32.00	3.3220	8.93
2.4244	-36.80	4.6990	7.37
3.0177	-38.60	5.9790	6.17

TABLE 4 (cont'd)

SOLUTION: 1.2% NATROSOL-250 G

τ_w, gm_f/cm^2	U_w, cm/sec	$\frac{8(<U>-U_w)}{D} \times 10^{-4}$, sec^{-1}	$\delta \times 10^4$, cm
.6220	-10.84	0.5500	17.84
1.2284	-19.40	1.3160	13.36
1.5306	-23.05	1.8250	11.40
1.8322	-26.20	2.3570	10.08
2.4508	-31.00	3.6100	7.77
3.0291	-33.80	4.9010	6.25

TABLE 5

Results for Capillary C

SOLUTION: 0.8% NATROSOL-250 G

τ_w, gm_f/cm^2	U_w, cm/sec	$\frac{8(<U>-U_w)}{D} \times 10^{-4}$, sec^{-1}	$\delta \times 10^4$, cm
1.0991	-19.52	2.4060	7.55
1.7485	-22.29	4.2520	4.96
2.6070	-15.96	6.9550	2.19
3.2443	- 3.91	8.9700	0.42
4.2920	+29.55	12.2440	0.86
5.3216	+78.96	15.1810	1.84

SOLUTION: 1.0% NATROSOL-250 G

τ_w, gm_f/cm^2	U_w, cm/sec	$\frac{8(<U>-U_w)}{D} \times 10^{-4}$, sec^{-1}	$\delta \times 10^4$, cm
1.1000	-17.80	1.6950	9.69
1.7517	-22.02	3.0860	6.59
2.6169	-20.08	5.1260	3.70
3.2613	-13.46	6.8080	1.90
4.3267	+ 7.94	9.5270	0.21
5.3787	+41.70	12.1630	0.89

TABLE 5 (cont'd).

SOLUTION: 1.2% NATROSOL-250 G

τ_w, gm_f/cm^2	U_w, cm/sec	$\frac{8(\langle U\rangle - U_w)}{D} \times 10^{-4}$, sec^{-1}	$\delta \times 10^4$, cm
1.1004	-15.50	1.2310	11.40
1.7532	-20.57	2.2720	8.20
2.6210	-22.53	3.9210	5.20
3.2701	-20.43	5.2870	3.50
3.9159	-15.33	6.7400	2.06
4.3449	-10.27	7.6810	1.21

TABLE 6

Results for Capillary D

SOLUTION: 0.8% NATROSOL-250 G

τ_w, gm_f/cm^2	U_w, cm/sec	$\frac{8(<U>-U_w)}{D} \times 10^{-4}$, sec^{-1}	$\delta \times 10^4$, cm
1.9791	- 2.10	4.9390	0.40
2.7572	+15.94	7.4180	0.71
3.5275	+44.33	9.8300	1.55
4.2890	+82.62	12.1120	2.38
4.7960	+113.78	13.7030	2.94

SOLUTION: 1.0% NATROSOL-250 G

τ_w, gm_f/cm^2	U_w, cm/sec	$\frac{8(<U>-U_w)}{D} \times 10^{-4}$, sec^{-1}	$\delta \times 10^4$, cm
1.9831	- 6.68	3.5470	1.75
2.9626	+ 8.70	5.9710	0.33
3.9332	+35.80	8.5830	1.05
4.8953	+74.80	10.9020	1.77
5.8457	+125.20	13.0940	2.47
6.7825	+186.00	15.4100	3.17

TABLE 6 (cont'd)

SOLUTION: 1.2% NATROSOL-250 G

τ_w, gm_f/cm^2	U_w, cm/sec	$\frac{8(<U>-U_w)}{D} \times 10^{-4}$, sec^{-1}	$\delta \times 10^4$, cm
1.5903	- 9.23	1.9220	4.35
2.7722	- 2.59	4.1080	0.57
3.5563	+ 8.14	5.8050	0.25
4.3363	+23.86	7.6070	0.61
4.7241	+33.54	8.5830	0.79

TABLE 7

Results for Capillary E

SOLUTION: 0.8% NATROSOL-250 G

τ_w, gm_f/cm^2	U_w, cm/sec	$\frac{8(<U>-U_w)}{D} \times 10^{-4}$, sec^{-1}	$\delta \times 10^4$, cm
1.5718	+ 23.90	3.9426	1.83
2.1935	+ 49.68	5.9340	2.79
2.8118	+ 84.46	7.7770	3.72
3.2733	+116.34	8.9950	4.38
3.7322	+153.14	10.1222	5.01

SOLUTION: 1.0% NATROSOL-250 G

τ_w, gm_f/cm^2	U_w, cm/sec	$\frac{8(<U>-U_w)}{D} \times 10^{-4}$, sec^{-1}	$\delta \times 10^4$, cm
2.6648	+ 52.20	5.3970	2.23
3.1321	+ 73.90	6.7500	2.72
3.9002	+118.00	8.8200	3.53
4.6663	+173.00	10.5000	4.31
5.4248	+238.00	12.2190	5.08
6.1796	+311.00	13.3290	5.75

TABLE 7 (cont'd)

SOLUTION: 1.2% NATROSOL-250 G

τ_w, gm_f/cm^2	U_w, $^{cm}/sec$	$\frac{8(<U>-U_w)}{D} \times 10^{-4}$, sec^{-1}	$\delta \times 10^4$, cm
1.5745	+ 8.59	1.8480	0.56
2.2002	+19.70	3.0030	0.95
2.8245	+35.17	4.3520	1.34
3.4472	+54.92	5.7620	1.75
3.7580	+66.42	6.3670	1.94

TABLE 8

Fluid Parameters

of Natrosol-250 G Solution

Concentration wt. %	Shear Stress Range gm_f/cm^2	n'	max. K $gm_f\text{-}sec^{n'}/cm^2$
0.6	0.461 - 4.641	0.739 - 0.921	4.50×10^{-4}
0.8	0.463 - 5.322	0.736 - 0.893	6.13×10^{-4}
1.0	0.464 - 6.783	0.751 - 0.959	7.11×10^{-4}
1.2	0.464 - 4.724	0.706	13.98×10^{-4}

lower Newtonian regime. Values of the fluid consistency index K' are different as the slope of the curve changes. In Table (8), the maximum value for K' is shown which is obtained at the lowest shear stress for the present experimental data.

According to equation (B-7) in Chapter 3, the slope of the straight line obtained in a plot of $8\langle U\rangle/D$ versus $8(\tau_w-\tau_c)/D^2$ for a particular concentration and value of τ_w should give the value of the modified slip coefficient $\alpha'(\tau_w)$. Figures (8, 9) show these plots for 1.0% and 1.2% Natrosol-250 G solutions. As expected, these plots were straight lines giving a constant α' for a particular value of τ_w. The points or lines located to the left of the origin (i.e. a negative $8(\tau_w-\tau_c)/D^2$) correspond to the polymer adsorption-gel formation phenomenon, whereas those located on the right side of the origin denote the separation phenomenon. For some τ_w, the transition points are also shown. The modified slip coefficient α' was found to increase linearly with the shear stress at the wall as shown in figure (10). The relationship between α' and τ_w can be represented by the simple equation $\alpha' = \alpha'' \tau_w$, where the slopes α'' were found to be equal to 0.22, 0.16 and 0.105 cm^6/gm_f^2-sec for 0.8%, 1.0% and 1.2% Natrosol-250 G solutions respectively.

An attempt was made to relate the critical shear stress to the diameter of the tube for different concentrations as shown in figure (12). It was found that the square of the critical shear stress might be approximated by a linear function of diameter. It is, however, interesting to note

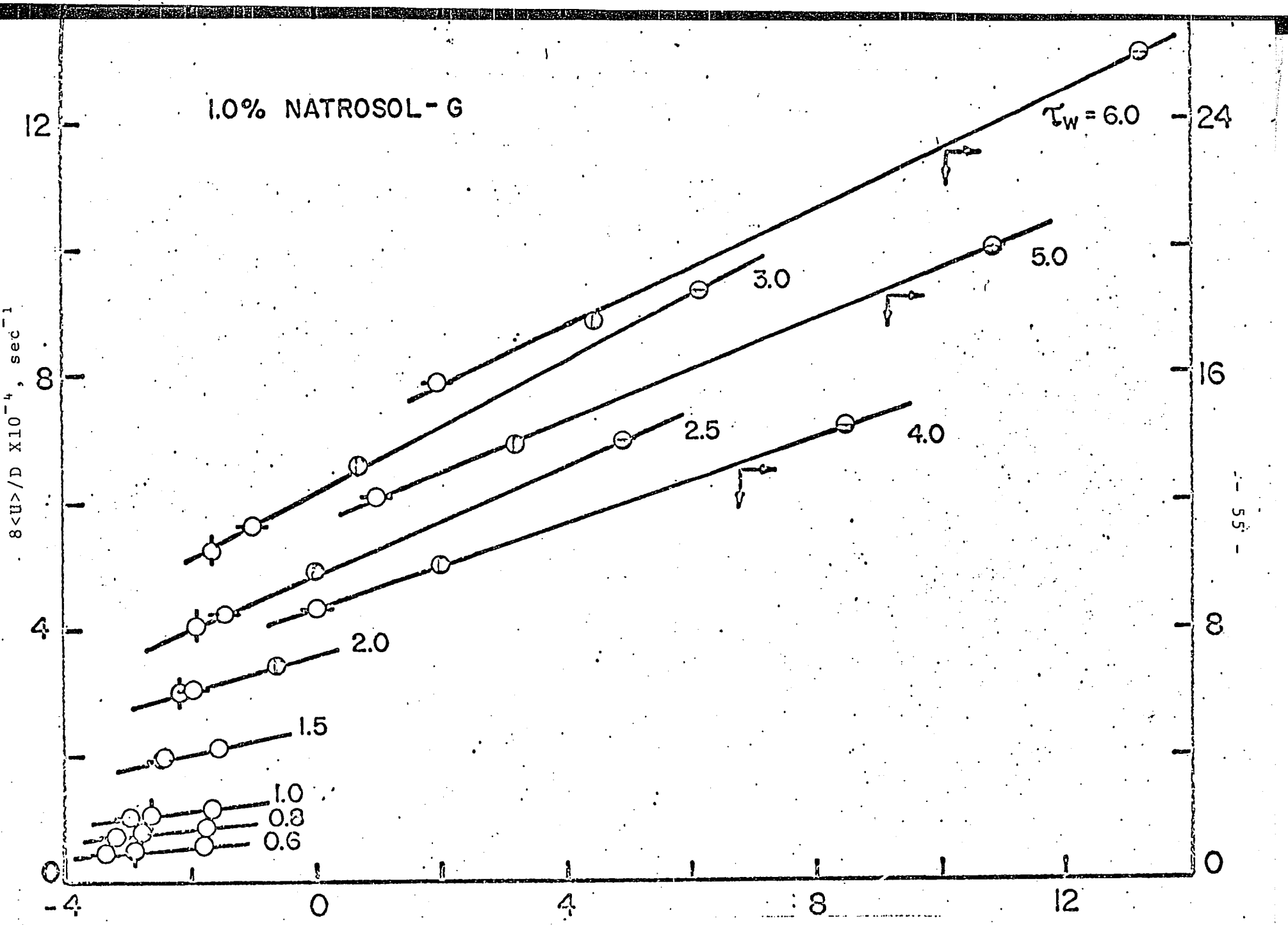

Figure 8. $8/D^2\{\tau_w - \tau_c\} \times 10^{-4}$, gm_f/cm^4.

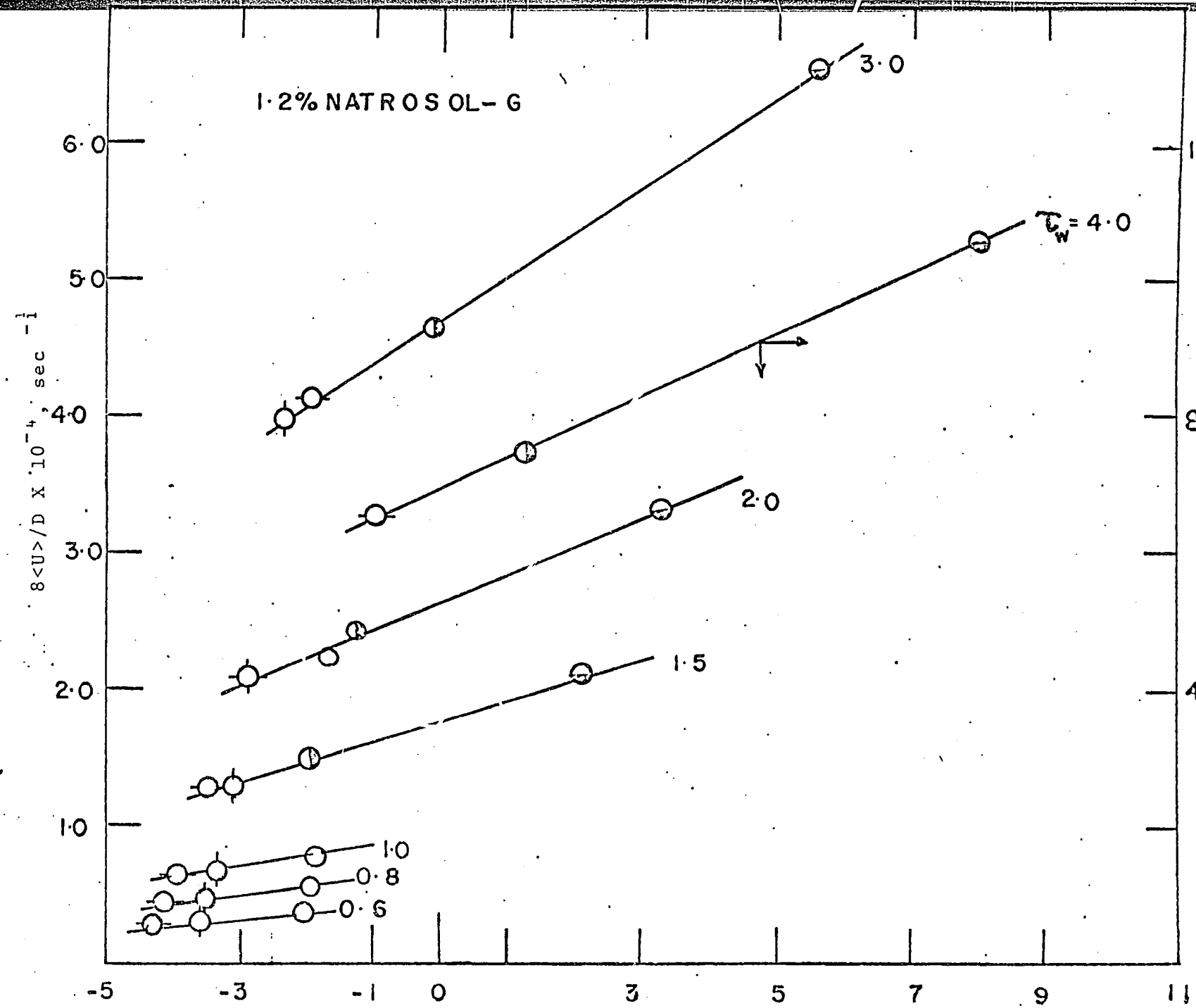

Figure 9. $8/D^2\{\tau_w - \tau_c\}$ X 10^{-4}, gm_f/cm^4

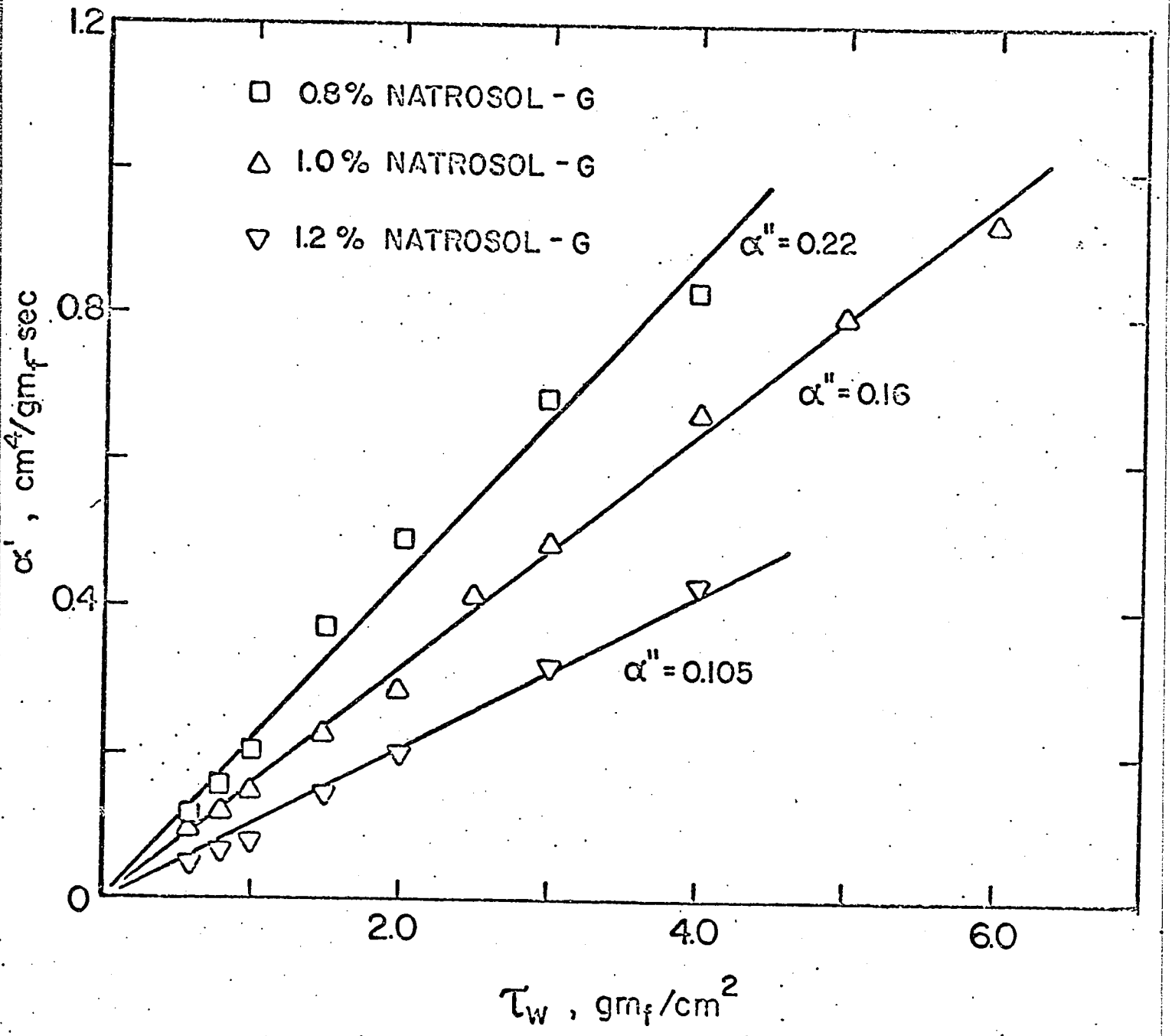

Figure 10. Plot of the Modified Slip Coefficient α' versus Shear Stress τ_w for Natrosol-250 G Solutions of Different Concentrations

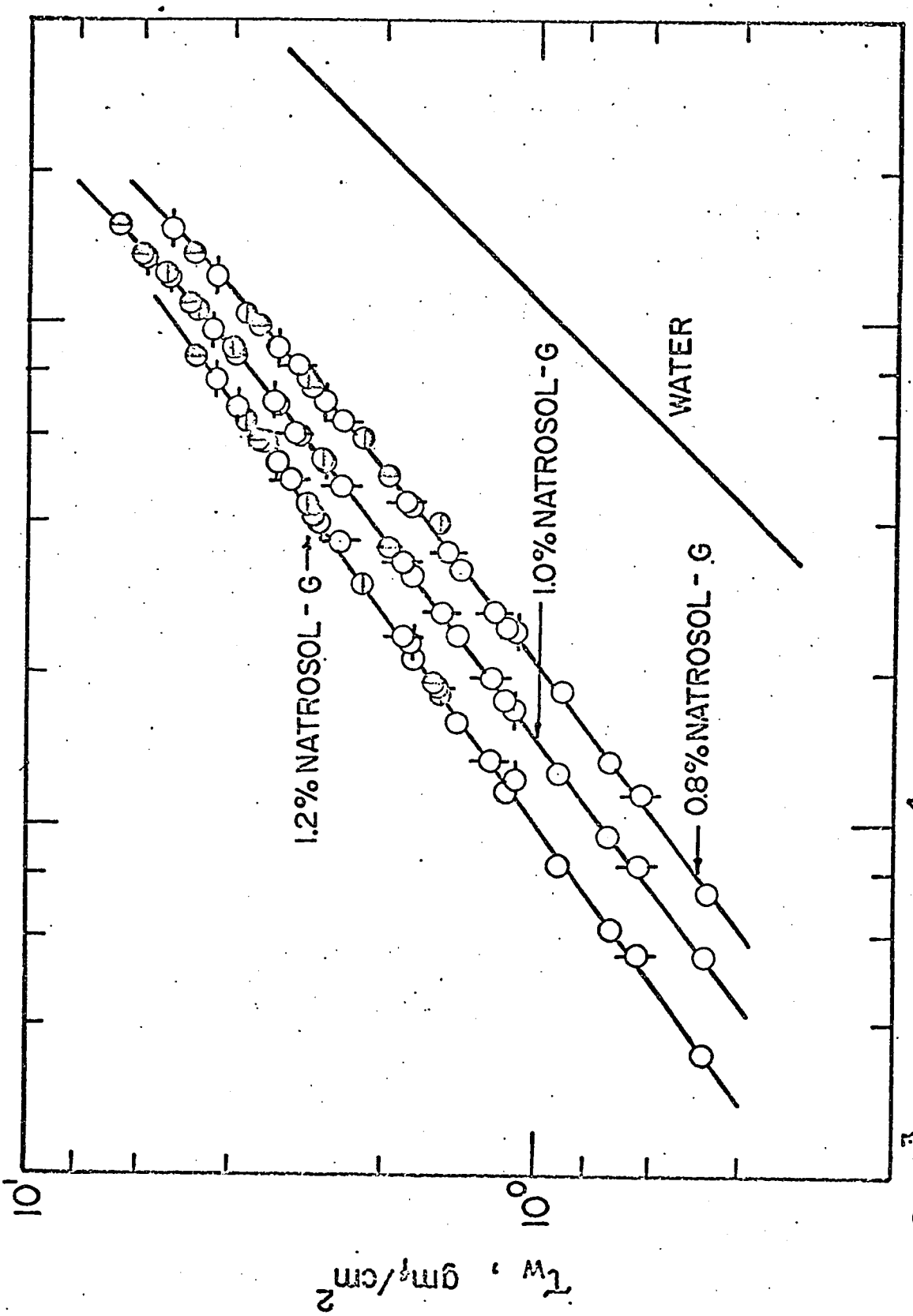

Figure 11. $8(\langle U\rangle - U_w)/D$ versus τ_w for Natrosol-250 G Solutions of Different Concentrations

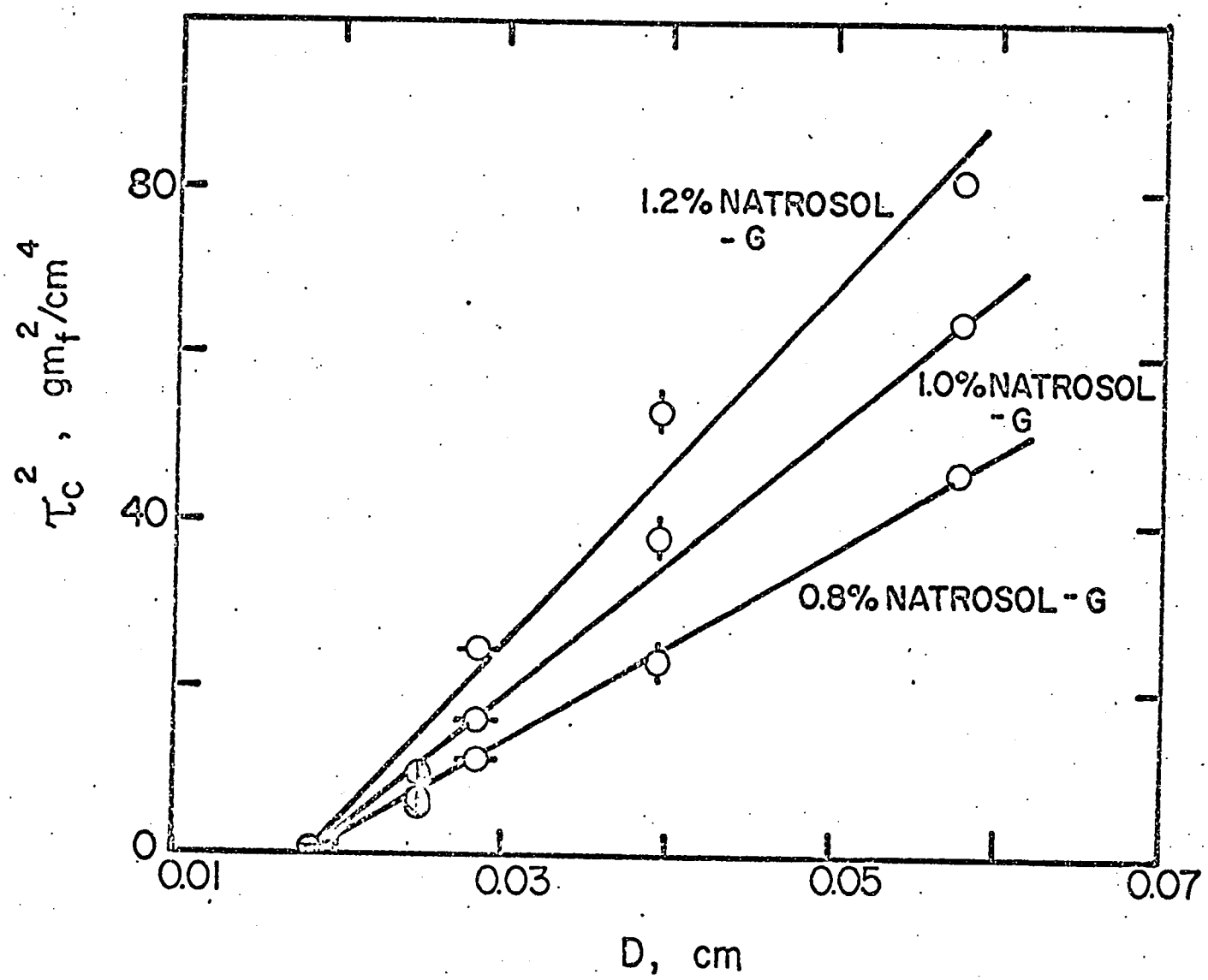

Figure 12: τ_c^2 versus D for Natrosol-250 G Solutions of Different Concentrations

that all the straight lines representing τ_c^2 versus D for various concentrations pass through a common intercept at a diameter of about 0.018 cm. This could be the value of the critical diameter below which the anomalous behavior of the fluid inside the tube could be mainly because of the polymer alignment. In other words, when the diameter of the capillary tube is smaller than this critical diameter, the size of the elongated molecule is significant in relation to the magnitude of the tube diameter. Therefore, the probability of the random orientation, as determined by the magnitude of the shear stress, of the polymer molecule inside the tube is reduced. The molecules tend to align themselves along the axis of the tube in order to pass through the capillary tube.

The anomalous layer thickness was calculated by means of equations (D-4, D-5) given in Chapter III. The results obtained for 0.8% Natrosol-250 G are shown in figure (13), plotted as a function of the shear stress. In the case of polymer adsorption-gel formation, the anomalous layer thickness decreases as the shear stress increases. The curves are extrapolated to intersect at the critical shear stresses on the abscissa where the anomalous layer thickness is zero. A thin layer of pure solvent is postulated to form near the tube wall when the applied shear stress is greater than the critical value, corresponding to the so-called separation phenomenon (1, 2). In this case, the anomalous layer thickness increases linearly with the shear stress and should

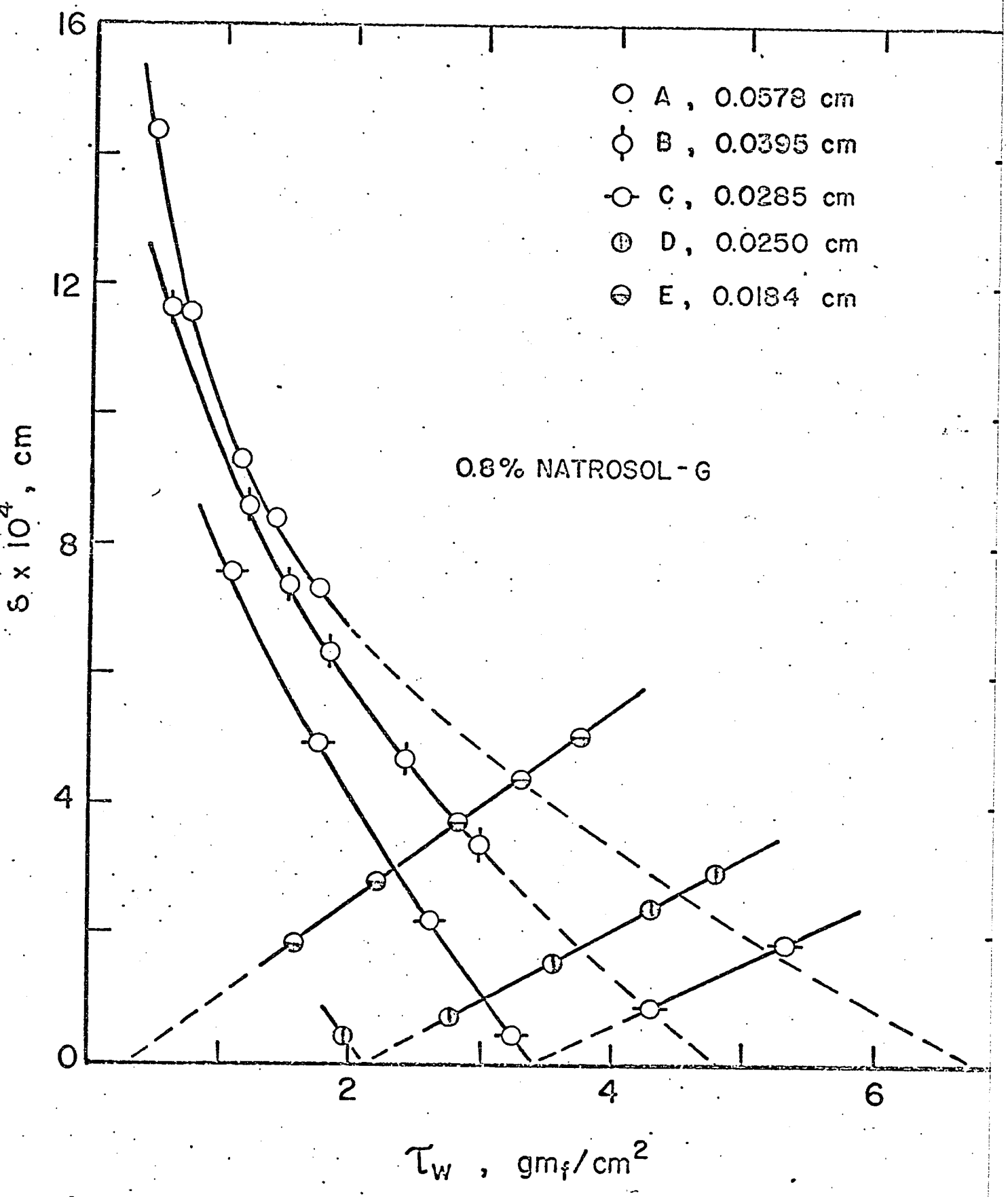

Figure 13. The Anomalous Layer Thickness δ versus Shear Stress τ_w for 0.8% Natrosol-250 G Solution for Tubes of Different Diameters

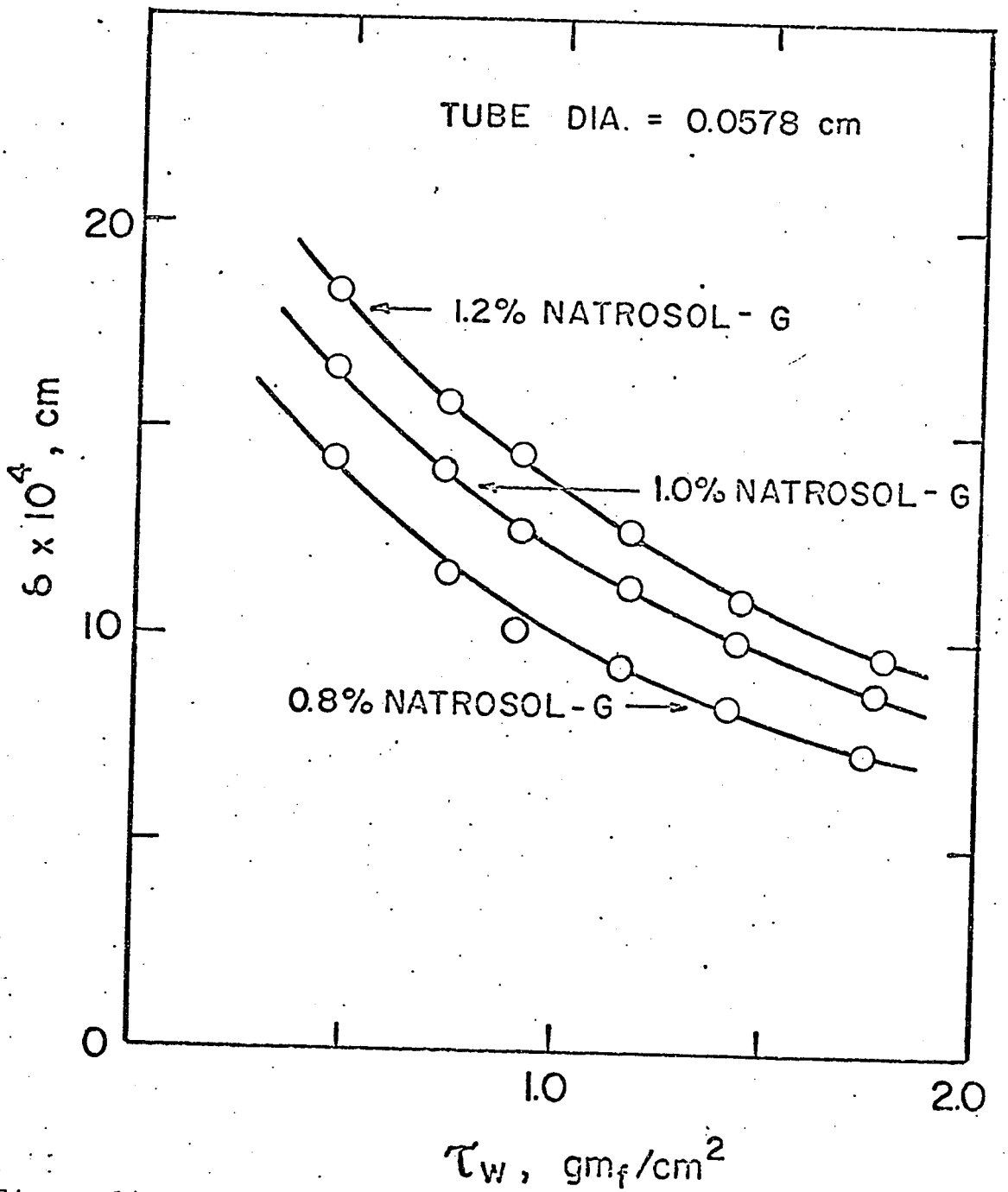

Figure 14. The Anomalous Layer Thickness δ versus Shear Stress τ_w for Natrosol-250 G Solutions of Different Concentrations for a Tube of 0.0578 cm. Diameter

approach a limiting value. The computed values of anomalous layer thickness are shown in the Tables (3, 4, 5, 6, 7). It is interesting to note that the maximum anomalous layer thickness attributable to polymer adsorption was obtained at the lowest shear stress and that attributable to separation at the highest shear stress. However, in both cases, the maximum δ/D ratio was always less than 5%. This is in conformity with the values of δ given by Astarita et al (2) for CMC solutions. Finally, figure (14) shows a plot of δ versus τ_w for polymer adsorption for three different Natrosol solutions in a particular tube A. As expected, the anomalous layer thickness is bigger for the solution of higher concentration at the same shear stress.

The data for the viscoelastic Natrosol-250 HR solutions which are presented remain to be analysed. The trend of the curves for various concentrations indicates that the same theory could be extended to explain the flow behavior of these solutions. For these solutions, time dependency was checked in Tubes A and C. For each tube diameter, two tubes of different lengths were taken keeping the L/D ratio above 400. A single curve resulted for different lengths of the same diameter as shown in the figure (15). Some data points for these solutions suggested the occurrence of premature turbulence which is found to be independent of concentration. This has also been reported by Sadowski and many other workers (46). No definite theoretical explanation could be given but it might be tentatively explained as a result of the

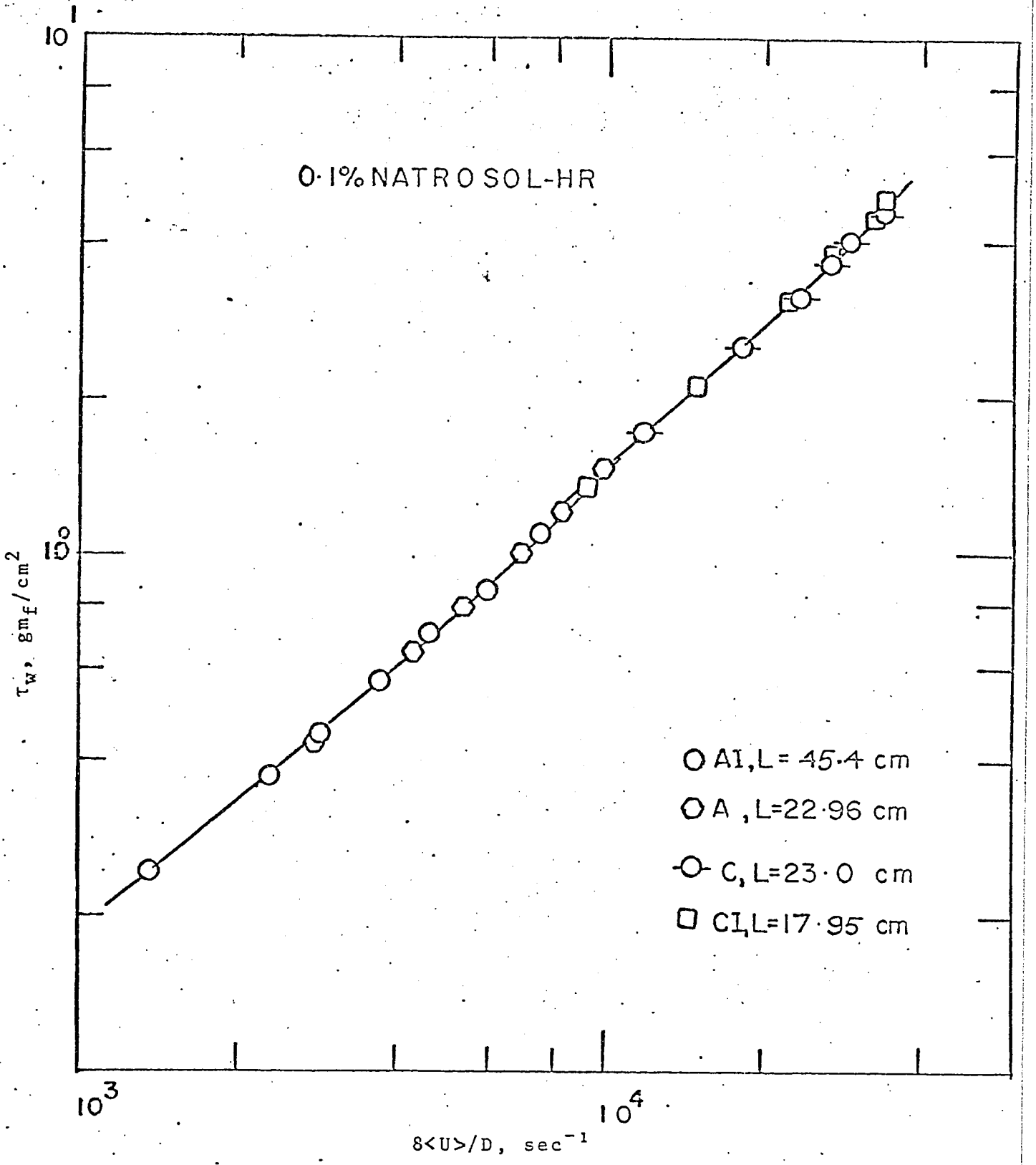

Figure 15. $8\langle U\rangle/D$ versus τ_w for 0.1% Natrosol-250 HR Solution at 25°C

local vibrations and unsteady flow conditions.

CHAPTER VII

DISCUSSION

The presentation of fundamental data usually requires a physical explanation of the observed phenomenon. In the present experimental work and subsequent analysis, significant information concerning the physical behavior of aqueous polymer solutions is deduced.

The flow behavior of aqueous polymer solutions has been the subject of both experimental and theoretical investigations by many workers. Most of the polymer solutions come under a broader class of fluids, namely pseudoplastics, characterized by the absence of a yield stress and continuous decrease of $\tau/\dot{\gamma}$ with increase of shear stress. The behavior of aqueous polymer solutions can be discussed separately under zero and low shear rates and under high shear rates. Certain polymer behavior can also be attributed to the transition region. Three main theories have been put forward to explain the behavior of polymer solutions at zero and low shear rates:

(a) Lodge and Goodeve (30, 20) have proposed that the network association of macromolecules predominates over the hydrodynamic effects of individual macromolecules. These theories necessarily predict the existence of a lower Newtonian regime. Studying the behavior of CMC and polyisobutylene solutions

in the lower shear range, Lodge (30) observed this Newtonian regime. His conclusions are further documented by the results of Phillipoff and others (9) on concentrated PIB solutions. In the present work, Natrosol solutions have a high degree of substitution. The molecules are non-electrolytic and are comprised of a large number of hydroxyl groups. Hence association into networks by hydrogen bonding is highly probable. But this may not be the only explanation for non-Newtonian behavior of these solutions. Another theory by Bueche (10) predicts that the pseudoplasticity in dilute solutions under moderate shear stress is due to the perturbation of the molecular configuration.

(b) Another qualitative theory, suggested by Merrill (1), postulates a random coil model to explain the behavior of macromolecules, non-electrolytic in solution, under low shear rates. His theory does not predict the first Newtonian regime. Molecular entanglement and interpenetration involving the solvent are predicted to take place at low shear rates. Molecular entanglements have also been reported by several other workers (23, 15).

(c) The third theory is based on polymer adsorption on the tube wall at multiple points of attachment. This phenomenon of polymer adsorption-gel formation has been reported by Sadowski and many other workers. Statistical mechanical approaches have been developed to explain the phenomenon theoretically. This adsorption gives rise to anomalous flow

behavior. This effect has been reported by Kozicki et al (28) in packed bed experiments involving CMC solutions. They have given quantitative values for the effective slip velocity at the solid surface to account for this adsorption phenomenon.

In the present work, the analysis, based on Oldroyd's theory, explains the behavior of flow curves determined for Natrosol solutions. The proposed theory does not rule out the possibility of the occurrence of polymer association and entanglement. The model takes into account all possible polymer behaviors in low shear rate region as evidenced by its successful use. A single flow curve results when corrections are applied based on this concept.

In an earlier chapter, the critical shear stress was introduced to determine the transition from adsorption to separation. The value for this critical shear decreases as the tube diameter decreases. For larger diameter tubes and low shear rate, adsorption is more likely to occur. For certain capillary diameters. there is a transition taking place from polymer adsorption to separation phenomenon, when the applied shear stress exceeds the critical shear stress. With an increase in shear rate and decrease in capillary diameter, molecules may uncoil and start orienting in the direction of flow. A pure solvent layer near the solid boundary starts to build up. The polymer behavior at high shear rate has been ascribed to similar causes by many workers.

The separation phenomenon has been observed by many

workers. Astarita (2) reported the formation of pure solvent layer near the solid wall for CMC solutions. The formation of clear water annulus in the pipe flow of pulp slurry has been demonstrated by Daily (14). Jastrzebski (25) obtained the same results for the flow of concentrated suspensions. An annulus solvent layer supposed to exist for Natrosol solutions is the possible cause of anomalous flow behavior at high shear rates. Furthermore, as the shear stress increases, the molecules are aligned more and more in the direction of flow. Supporting evidence has been put forward by many workers (12, 41, 55). Staudinger (55) postulates that the shear couples caused by the flow tend to orient the particles with their long axis parallel to the direction of flow in contrast to the completely random positions existing under static conditions. The tendency towards orientation increases with the rate of shear. The present experimental evidence also confirms the theoretical predictions of Peterlin (41), describing ultimate complete extension of the macromolecules in the direction of flow.

It is seen that all these effects could be easily accounted for by calculating an effective slip velocity. Furthermore, a single rheological curve is obtained after applying this correction. The present work also shows that the second Newtonian regime could begin around a shear rate value of $2X10^4$ to 10^5 sec^{-1}. This has been earlier predicted by Merrill and other workers (1).

CHAPTER VIII

CONCLUSION

An explanation of the behavior of high molecular weight aqueous polymer solutions has been offered. This study is by no means exhaustive. Significant work has been conducted on low molecular weight polymers elsewhere. The behavior of concentrated polymer solutions and molten polymers has also been interpreted and explained by several workers. In the present study of aqueous polymer solutions, some of the results are in agreement with the previous work. It is felt the additional findings provide an important contribution in the understanding of the flow behavior of aqueous polymer solutions. The conclusions can be summarized in general as follows:

(a) The results indicate a greater wall effect with smaller tube diameter because of the proportionally greater amount of fluid under the influence of the wall. This has also been predicted by other workers (25, 55, 39). So the true rheological curve is closer to the curve for the largest diameter capillary tube in high as well as low shear rates. Harper and Morrison (37) noticed similar effects in Couette flow.

(b) The discrepancies between the flow curves are also functions of the shear rate. According to Jastrzebski (25), for concentrated suspensions the discrepancies are greater

in the region of low shear rate than at high shear rates. In the present study, however, these discrepancies in both regions were found to be comparable. The flow characteristics are attributable to different flow behavior in the two regions. In the lower shear rate region, the separation of the flow curves is ascribed to polymer adsorption and entanglement. In the high shear rate region, formation of a solvent layer near the solid wall and orientation of molecules in the direction of flow has been proposed.

(c) The present study predicts the existence of a critical shear stress which marks the transition in the fluid behavior from polymer adsorption to the separation phenomenon at the wall. This critical shear stress decreases with decrease in the diameter of tube.

(d) The possibility of the existence of a critical tube diameter below which only polymer alignment is the cause of the anomalous flow behavior is suggested. The value of the critical tube diameter is independent of the concentration of the polymer solution.

(e) Depending on the molecular structure, several empirical relations (3) have been suggested to predict the viscosity of polymer solutions. These do not account for the anomalous flow behavior. It is reasonable to suggest that if this behavior is considered, more reliable viscosity values will be determined from viscometric measurements. The dependence of viscosity on molecular weight and structure is of significance. Therefore the viscometric measurements

could give some information about the molecular characteristics after the corrections for anomalous flow behavior have been made.

NOMENCLATURE

a, b = geometric coefficients, dimensionless.

D = Diameter of the Capillary Tube, cm.

$\frac{\bar{D}}{Dt}$ = Jaumann derivative, sec^{-1}.

f_c = Critical friction factor, dimensionless.

g = Acceleration due to gravity, cm/sec^2

g_c = Newton's law conversion factor, $gm\text{-}cm/gmf\text{-}sec^2$

K = Fluid consistency index for Power-law fluid,
= $gmf\ sec^n/cm^2$.

K' = Fluid consistency index, $gmf\ sec^{n'}/cm^2$.

K^* = Generalized fluid consistency index, $gmf\ sec^{n^*}/cm^2$.

K_c = Entrance losses correction factor.

L = Length of the capillary tube, cm.

L' = Liquid head above the capillary exit, cm.

m = Constant in the Power-law model, gm/cm-sec.

n = Flow behavior index for Power-law fluid, dimensionless.

n' = Dimensionless index for circular conduits.

n^* = Generalized flow behavior index, dimensionless.

$\bar{n}$ = Outward normal, cm.

P_a = Atmospheric pressure, gmf/cm^2

P_{gas} = Pressure applied by gas, gmf/cm^2

ΔP = Pressure drop across the capillary tube, gmf/cm^2.

q = Constant in the Meter model, dimensionless.

r_H = Hydraulic radius, cm.

Re = Reynolds number, dimensionless.

Re_c = Critical Reynolds number, dimensionless.

r, y = Radial distance from the wall, cm.

u = Local point velocity in axial direction, cm/sec.

$\langle U \rangle$ = Average velocity, cm/sec.

U_w = Effective slip velocity at the wall, cm/sec.

α = Kinetic energy correction factor, dimensionless.

α' = Slip coefficient, $cm^4/gmf\text{-}sec$.

α'' = Modified slip coefficientm $cm^6/gmf^2\text{-}sec$.

β = Normal stress function associated with $\tau_{22} - \tau_{33}$.

$\dot{\gamma}, \Delta$ = Rate of strain tensor, sec^{-1}.

ξ = Slip coefficient, $cm^3/gmf\text{-}sec$.

η, η' = Non-Newtonian viscosity, $gmf\text{-}sec/cm^2$

η_o = Lower limiting viscosity, $gmf\text{-}sec/cm^2$

η_∞ = Upper limiting viscosity, $gmf\text{-}sec/cm^2$.

θ = Normal stress function associated with $\tau_{11} - \tau_{22}$.

λ_c = Stability parameter, dimensionless

ρ = Density, gm/cm^3.

δ = Anomalous layer thickness, cm.

μ_s = Solvent viscosity, $gmf\text{-}sec/cm^2$.

τ = Shear stress, gmf/cm^2.

τ_c = Critical shear stress, gmf/cm^2

τ_m = Constant in the Meter model, gmf/cm^2.

τ_w = Shear stress at the wall, gmf/cm^2.

REFERENCES

1. Acrivos, A., "Modern Chemical Engg.", Vol. I, chapter by Merrill, E.W., "Non-Newtonianism in Thin Liquids", Reinhold, New York, 1963.

2. Astarita, G., Marrucci, G. and Palumbo, G., I & EC Fundls, 3, 333 (1964).

3. Badgley, W.J., and Mark, H. "Osmometry and Viscosity" in "High molecular weight Organic Compounds", edited by Burk, R.E., Interscience, New York, 1949.

4. Bagley, E.B., J. Appl. Phys., 28, 624 (1957).

5. Bingham, E.C., and Green, H., Proc. Am. Soc. Testing Materials, 19, 640 (1919).

6. Bird, R.B., Stewart, W.E., and Lightfoot, E.N., "Transport Phenomena", John Wiley & Sons, Inc., New York, 1960.

7. Bogue, D.C., and Doughty, J.O., Ind. Eng. Chem. Fundamentals, 5, 243 (1966).

8. Bowen, R.L., Chemical Engg., Aug. 21 (1961).

9. Brodnyan, J.G., Gaskins, F.H., Philippoff, W., Trans. Soc. Rheol., 1, 109 (1957).

10. Bueche, F., J. Chem. Phys., 22, 1570 (1954).

11. Carreau, P.J., and Bird, R.B., Chem. Engg. Sc., 23, 427 (1968).

12. Claesson, S., and Lohmander, U., Makromolekulare Chemie, 44-46, 461 (1961).

13. Coleman, B.D., and Noll, W., J. Appl. Phys., 30, 1508 (1959).

14. Daily, J.W., and Bugliarello, G., M.I.T. Hydromechanics Lab. Report No. 30, Dept. of Civil Engg., Oct. 1958.

15. Davies, C.N., Proc. Int. Congress on Rheology, II-152, Scheveningen (Holland), 1948.

16. Eirich, F.R., "Rheology", Vol. I, Chapter by Oldroyd, J.G., "Non-Newtonian Flow of Liquids and Solids", Academic, New York, 1956.

17. Ericksen, J.L., Trans. Soc. Rheol., 4, 29 (1960).

18. Foust, A.S., et al, "Principles of Unit Operations", John Wiley & Sons, New York, 1960.

19. Frish, H.L., Hellman, M.Y., and Lundberg, J.L., J. Polymer Sci., 38, 441 (1959).

20. Goodeve, C.F., Trans. Faraday Soc., 35, 342 (1935).

21. Goring, D.A., and Sitaramaiah, G., Polymer, 4, 7 (1963).

22. Green, A. E., and Rivlin, R.S., Arch. Ratl. Mech. Anal., 4, 387 (1960).

23. Haas, H.C., Journal of Polymer Sci., 17, 135 (1955).

24. Hobden, J.F., and Jellinek, H.H.G., J. Polymer Sci., 11, 365 (1953).

25. Jastrzebski, Z.D., I & EC Fundamentals, 3, 445 (1967).

26. Koral, J., Ullman, R., and Eirich, F.R., J. Phys. Chem., 62, 541 (1958).

27. Kozicki, W., Chou, C.H., and Tiu, C., Chem. Engg. Sci., 21, 665 (1966).

28. Kozicki, W., Hsu, C.J., and Tiu, C., Chem. Engg. Sci., 22, 487 (1967).

29. Kozicki, W., and Tiu, C., Chem. Engg. Sci., 23, 231 (1968).

30. Lodge, A.S., Trans. Faraday Soc., 52, 120 (1956).

31. Luce, J.E., and Robertson, A.A., J. Polymer Sci., 51, 317 (1961).

32. Merrill, E.W., Ind. & Eng. Chem., 51, 868 (1959).

33. Meter, D.M., Ph.D. Thesis, University of Wisconsin, 1963.

34. Meter, D.M., A.I.Ch. E. Jl., 10, 881 (1964).

35. Metzner, A.B., and Reed, J.C., A.I.Ch.E.Jour., 1. 434,(1955).

36. Mooney, M., J. Rheol., 2, 210 (1931).

37. Morrison, S.R., and Harper, J.C., I & EC Fundamentals, 4, 176 (1965).

38. Noll, W., Arch. Ratl. Mech. Anal., 2, 197 (1958).

39. Oldroyd, J.G., J. Colloid Sci., 4, 333 (1949).

40. Oldroyd, J.G., Rheologica Acta, 1, 337 (1961).

41. Peterlin, A., Makromolekulare Chemie, 44-46, 338 (1961).

42. Rabinowitsch, B., Z. Phys. Chem., 1, A 145 (1929).

43. Reiner, M., "Deformation, Strain and Flow", Interscience, New York, 1960.

44. Rivlin, R.S., and Ericksen, J.L., J. Ratl. Mech. Anal., 4, 323 (1955).

45. Rouse, P.E., J. Chem. Phys., 21, 1272 (1953).

46. Sadowski, T.J., Ph.D. Thesis, University of Wisconsin (1963).

47. Schofield, R.K., and Blair, G.W.S., J. Phys. Chem., 34, 248, (1930); 35, 1212 (1931).

48. Severs, E.T., and Austin, J.M., I & EC, 46, 2369 (1954).

49. Skelland, A.H.P., "Non-Newtonian Flow and Heat Transfer", John Wiley & Sons, New York, 1967.

50. Spriggs, T.W., and Bird, R.B., Ind.& Eng. Chem. Fundamentals, 4, 182 (1965).

51. Toms, B.A., Proc. Ist. Intern. Cong. Rheology, Holland, 1948.

52. Toms, B.A., J. Colloid Sci., 4, 511 (1949).

53. Toor, H.L., Trans. Soc. Rheol., 1, 177 (1957).

54. Van Wazer, J.R., Lyons, J.W., Kim, K.Y., and Colwell, R.E., "Viscosity and Flow Measurements", Interscience, New York, (1963).

55. Winding, C.C., Baumann, G.P., and Kranich, W.L., Chem. Engg. Prog., 43, 527 (1947).

56. Yurzhenko, A.L., and Maleyev, L.L., J. Polymer Sci., 31, 301 (1958).

57. Zimm, B.H., J. Chem. Phys., 24, 269 (1956).

APPENDIX I

SUMMARY OF VISCOMETRIC RESULTS*

FOR NATROSOL-250 G AND HR SOLUTIONS

* All the measurements were taken at 25° C.

TABLE: 1

CAPILLARY TUBE SPECIFICATIONS

CAPILLARY	LENGTH, L, IN CM	CALI. DIAM. D, IN CM	L/D
A	22.96	.0578	397.23
AI	45.40	.0578	785.47
B	22.90	.0395	579.74
C	23.00	.0285	807.01
CI	17.95	.0285	629.82
D	20.37	.0250	814.80
DI	22.28	.0250	891.20
E	20.66	.0184	1,122.82

TABLE: 2

SOLUTION: 0.6% (BY WT.) NATROSOL-250 G

DENSITY OF SOLUTION: 1.0159 gm/cm^3 at 25°C

DATA FOR CAPILLARY A

ΔP, PSIG	W, gm/sec.	$\frac{8\langle U\rangle}{D} \times 10^{-4}$, sec^{-1}	τ_w, gm_f/cm^2
10	.1783	.9219	.4610
16	.3333	1.7237	.7175
20	.4392	2.2710	.8851
26	.5999	3.1023	1.1365
32	.7666	3.9641	1.3778
40	.9852	5.0944	1.6919

DATA FOR CAPILLARY B

ΔP, PSIG	W, gm/sec.	$\frac{8\langle U\rangle}{D} \times 10^{-4}$, sec^{-1}	τ_w, gm_f/cm^2
20	.0878	1.4206	.6197
40	.2098	3.3931	1.2149
50	.2791	4.5133	1.5070
60	.3617	5.8483	1.7930
80	.5208	8.4208	2.3583
100	.6753	10.9186	2.9059

DATA FOR CAPILLARY C

ΔP, PSIG	W, gm/sec.	$\frac{8\langle U\rangle}{D} \times 10^{-4}$, sec^{-1}	τ_w, gm_f/cm^2
50	.0653	2.8196	1.0970
80	.1225	5.2895	1.7417
120	.2103	9.0845	2.5886
150	.2786	12.0330	3.2140
170	.3271	14.1278	3.6247
200	.3993	17.2445	4.2338

DATA FOR CAPILLARY D

ΔP, PSIG	W, gm/sec.	$\frac{8\langle U\rangle}{D} \times 10^{-4}$, sec^{-1}	τ_w, gm_f/cm^2
50	.0466	2.9691	1.0882
80	.0876	5.5793	1.7292
100	.1154	7.3434	2.1536
150	.1897	12.0755	3.2030
200	.2665	16.9616	4.2348
220	.2989	19.0205	4.6413

DATA FOR CAPILLARY E

ΔP, PSIG	W, gm/sec.	$\frac{8\langle U\rangle}{D} \times 10^{-4}$, sec^{-1}	τ_w, gm_f/cm^2
60	.0223	3.5775	.9461
100	.0439	7.0332	1.5681
150	.0757	12.1222	2.3386
180	.0958	15.3414	2.7967
220	.1236	19.7876	3.4023
242	.1398	22.3947	3.7320

TABLE: 3

SOLUTION: 0.8% NATROSOL-250 G

DENSITY OF SOLUTION: 1.01633 gm/cm^3

DATA FOR CAPILLARY A

ΔP, PSIG	W, gm/sec.	$\frac{8\langle U\rangle}{D} \times 10^{-4}$, sec^{-1}	τ_w, gm_f/cm^2
10	.1099	.5682	.4630
16	.2161	1.1174	.7248
20	.3041	1.5720	.8967
26	.4147	2.1438	1.1538
32	.5503	2.8446	1.4083
40	.7485	3.8693	1.7358

DATA FOR CAPILLARY B

ΔP, PSIG	W, gm/sec	$\frac{8\langle U\rangle}{D} \times 10^{-4}$, sec^{-1}	τ_w, gm_f/cm^2
20	.0534	.8637	.6212
40	.1337	2.1612	1.2237
50	.1864	3.0124	1.5217
60	.2408	3.8931	1.8177
80	.3617	5.8461	2.4017
100	.4858	7.8516	2.9752

DATA FOR CAPILLARY C

ΔP, PSIG	W, gm/sec.	$\frac{8\langle U\rangle}{D} \times 10^{-4}$, sec^{-1}	τ_w, gm_f/cm^2
50	.0430	1.8578	1.0991
80	.0839	3.6262	1.7485
120	.1507	6.5065	2.6070
150	.2052	8.8595	3.2443
200	.3028	13.0727	4.2920
250	.4029	17.3966	5.3216

DATA FOR CAPILLARY D

ΔP, PSIG	W, gm/sec	$\frac{8\langle U\rangle}{D} \times 10^{-4}$, sec^{-1}	τ_w, gm_f/cm^2
100	.0766	4.8719	1.9791
140	.1246	7.9275	2.7572
180	.1768	11.2487	3.5275
220	.2320	14.7560	4.2890
247	.2727	17.3444	4.7960

DATA FOR CAPILLARY E:

ΔP, PSIG	W, gm/sec.	$\frac{8\langle U\rangle}{D} \times 10^{-4}$, sec^{-1}	τ_w, gm_f/cm^2
100	.0311	4.9811	1.5718
140	.0505	8.0935	2.1935
180	.0715	11.4488	2.8118
210	.0877	14.0529	3.2733
240	.1049	16.7966	3.7322

TABLE: 4

SOLUTION: 1.0% (BY WT.) NATROSOL-250 G

DENSITY OF SOLUTION: 1.01695 gm/cm^3

DATA FOR CAPILLARY A:

ΔP, PSIG	W, gm/sec.	$\frac{8\langle U\rangle}{D} \times 10^{-4}$, sec^{-1}	τ_w, gm_f/cm^2
10	.0795	.4109	.4636
16	.1453	.7507	.7274
20	.2005	1.0361	.9021
26	.2858	1.4767	1.1631
32	.3903	2.0163	1.4211
40	.5321	2.7590	1.7656

DATA FOR CAPILLARY B:

ΔP, PSIG	W, gm/sec.	$\frac{8\langle U\rangle}{D} \times 10^{-4}$, sec^{-1}	τ_w, gm_f/cm^2
20	.0341	.5517	.6218
40	.0900	1.4537	1.2269
50	.1271	2.0536	1.5277
60	.1655	2.6736	1.8276
80	.2448	3.9540	2.4244
100	.3218	5.1983	3.0177

DATA FOR CAPILLARY C:

ΔP, PSIG	W, gm/sec	$\frac{8\langle U\rangle}{D} \times 10^{-4}$, sec^{-1}	τ_w, gm_f/cm^2
50	.0277	1.1947	1.1000
80	.0572	2.4672	1.7517
120	.1057	4.5617	2.6169
150	.1490	6.4298	3.2613
200	.2259	9.7497	4.3267
250	.3091	13.3383	5.3787

DATA FOR CAPILLARY D:

ΔP,PSIG	W, gm/sec.	$\frac{8\langle U\rangle}{D} \times 10^{-4}$, sec^{-1}	τ_w, gm_f/cm^2
100	.0524	3.3326	1.9831
150	.0983	6.2500	2.9626
200	.1530	9.7286	3.9332
250	.2092	13.2970	4.8953
300	.2705	17.1935	5.8457
350	.3362	21.3695	6.7825

DATA FOR CAPILLARY E:

ΔP, PSIG	W, gm/sec.	$\frac{8\langle U\rangle}{D} \times 10^{-4}$, sec^{-1}	τ_w, gm_f/cm^2
170	.0479	7.6670	2.6648
200	.0623	9.9664	3.1321
250	.0872	13.9595	3.9002
300	.1126	18.0207	4.6663
350	.1411	22.5688	5.4248
400	.1678	26.8392	6.1796

TABLE: 5

SOLUTION: 1.2% NATROSOL-250 G

DENSITY OF SOLUTION: 1.0175 gm/cm^3

DATA FOR CAPILLARY A:

ΔP, PSIG	W, gm/sec.	$\frac{8\langle U\rangle}{D} \times 10^{-4}$, sec^{-1}	τ_w, gm_f/cm^2
10	.0481	.2486	0.4641
16	.0908	.4692	0.7287
20	.1229	.6348	0.9046
26	.1818	.9388	1.1681
32	.2571	1.3277	1.4300
40	.3555	1.8353	1.7777

DATA FOR CAPILLARY B:

ΔP, PSIG	W, gm/sec.	$\frac{8\langle U\rangle}{D} \times 10^{-4}$, sec^{-1}	τ_w, gm_f/cm^2
20	.0204	.3304	0.6220
40	.0571	.9226	1.2284
50	.0840	1.3569	1.5306
60	.1131	1.8266	1.8322
80	.1847	2.9815	2.4508
100	.2612	4.2165	3.0291

DATA FOR CAPILLARY C:

ΔP, PSIG	W, gm/sec.	$\frac{8\langle U\rangle}{D} \times 10^{-4}$, sec^{-1}	τ_w, gm_f/cm^2
50	.0184	0.7964	1.1004
80	.0393	1.6951	1.7532
120	.0762	3.2882	2.621
150	.1093	4.7128	3.2701
180	.1463	6.3098	3.9159
200	.1714	7.3932	4.3449

DATA FOR CAPILLARY D:

ΔP, PSIG	W, gm/sec.	$\frac{8\langle U\rangle}{D} \times 10^{-4}$, sec^{-1}	τ_w, gm_f/cm^2
80	.0256	1.6265	1.5903
140	.0633	4.0248	2.7722
180	.0954	6.0645	3.5563
220	.1317	8.3712	4.3363
240	.1520	9.6561	4.7241

DATA FOR CAPILLARY E:

ΔP, PSIG	W, gm/sec.	$\frac{8\langle U\rangle}{D} \times 10^{-4}$, sec^{-1}	τ_w, gm_f/cm^2
100	.0139	2.2215	1.5745
140	.0241	3.8603	2.2002
180	.0367	5.8814	2.8245
220	.0509	8.1500	3.4472
240	.0579	9.2549	3.7580

TABLE: 6

SOLUTION: 0.1% NATROSOL-250 HR

DENSITY OF SOLUTION: 1.01438 gm/cm^3

DATA FOR CAPILLARY A:

ΔP, PSIG	W, gm/sec.	$\frac{8\langle U\rangle}{D} \times 10^{-4}$, sec^{-1}	τ_w, gm_f/cm^2
10	.5422	2.8079	.4341
16	.8365	4.3324	.6571
20	1.0479	5.4270	.7923
26	1.3271	6.8731	.9927
32	1.5734	8.1487	1.1841
40	1.8898	9.7874	1.4250

DATA FOR CAPILLARY AI:

ΔP, PSIG	W, gm/sec.	$\frac{8\langle U\rangle}{D} \times 10^{-4}$, sec^{-1}	τ_w, gm_f/cm^2
10	.2613	1.3533	.2385
16	.4402	2.2798	.3648
20	.5410	2.8019	.4509
26	.7128	3.6918	.5736
32	.8877	4.5973	.6929
40	1.1311	5.8582	.8461

DATA FOR CAPILLARY B:

ΔP, PSIG	W, gm/sec.	$\frac{8\langle U\rangle}{D} \times 10^{-4}$, sec^{-1}	τ_w, gm_f/cm^2
20	.2427	3.9304	.6032
40	.4853	7.8584	1.1533
50	.6084	9.8520	1.4130
60	.7191	11.6444	1.6688
80	.9456	15.3129	2.1580
100	1.1157	18.0672	2.6522

DATA FOR CAPILLARY C:

ΔP, PSIG	W, gm/sec.	$\frac{8\langle U\rangle}{D} \times 10^{-4}$, sec^{-1}	τ_w, gm_f/cm^2
50	.2140	9.2572	1.3596
80	.3452	14.9308	2.1165
120	.5074	21.9474	3.0818
150	.6229	26.9434	3.7762
180	.7465	32.2920	4.4283
200	.7748	33.5142	4.9391

DATA FOR CAPILLARY CI:

ΔP, PSIG	W, gm/sec.	$\frac{8\langle U\rangle}{D} \times 10^{-4}$, sec^{-1}	τ_w, gm_f/cm^2
50	.1728	7.4762	1.0751
80	.2795	12.0897	1.6877
120	.4132	17.8720	2.4804
150	.5303	22.9379	3.0398
180	.6172	26.6993	3.6097
200	.6738	29.1454	3.9830

DATA FOR CAPILLARY D:

ΔP, PSIG	W, gm/sec.	$\frac{8\langle U\rangle}{D} \times 10^{-4}$, sec^{-1}	τ_w, gm_f/cm^2
80	.1914	12.1970	1.5436
100	.2476	15.7788	1.9067
150	.3706	23.6185	2.7964
200	.4969	31.6724	3.6423
250	.3054	19.4650	4.8316
300	.3281	20.9097	5.8014

DATA FOR CAPILLARY E:

ΔP, PSIG	W, gm/sec.	$\frac{8\langle U\rangle}{D} \times 10^{-4}$, sec^{-1}	τ_w, gm_f/cm^2
100	.0989	15.8646	1.5406
150	.1489	23.8799	2.2808
180	.1833	29.4068	2.7106
200	.2008	32.2063	3.0004
250	.2470	39.6192	3.7113
300	.2928	46.9654	4.4079

TABLE: 7

SOLUTION: 0.2% NATROSOL- 250 HR

DENSITY OF SOLUTION: 1.01494 gm/cm^3

DATA FOR CAPILLARY A:

ΔP, PSIG	W, gm/sec.	$\frac{8\langle U\rangle}{D} \times 10^{-4}$, sec^{-1}	τ_w, gm_f/cm^2
10	.3579	1.8529	.4509
16	.6068	3.1410	.6892
20	.7815	4.0449	.8447
26	.9981	5.1662	1.0681
32	1.2401	6.4186	1.2815
40	1.5734	8.1438	1.5370

DATA FOR CAPILLARY B:

ΔP, PSIG	W, gm/sec.	$\frac{8\langle U\rangle}{D} \times 10^{-4}$, sec^{-1}	τ_w, gm_f/cm^2
20	.1573	2.5460	.6144
40	.3507	5.6757	1.1892
50	.4663	7.5472	1.4614
60	.5563	9.0036	1.7384
80	.7718	12.4920	2.2529
100.	.9644	15.6076	2.7894

DATA FOR CAPILLARY C:

ΔP, PSIG	W, gm/sec.	$\frac{8\langle U\rangle}{D} \times 10^{-4}$, sec^{-1}	τ_w, gm_f/cm^2
50	.1189	5.1427	1.0887
80	.2076	8.9778	1.7178
120	.3294	14.2399	2.5338
150	.4137	17.8839	3.1342
203	.5608	24.2459	4.1801
250	.6898	29.8210	5.0554

DATA FOR CAPILLARY D:

ΔP, PSIG	W, gm/sec.	$\frac{8\langle U\rangle}{D} \times 10^{-4}$, sec^{-1}	τ_w, gm_f/cm^2
80	.1492	9.5006	1.7088
150	.3058	19.4776	3.1215
200	.4107	26.1612	4.0959
260	.5366	34.1783	5.2240
320	.6611	42.1078	6.3592
350	.7224	46.0132	6.8402

DATA FOR CAPILLARY E:

ΔP, PSIG	W, gm/sec.	$\frac{8\langle U\rangle}{D} \times 10^{-4}$, sec^{-1}	τ_w, gm_f/cm^2
100	.0665	10.6684	1.4415
150	.1053	16.8843	2.1440
200	.1484	23.7959	2.8327
250	.1883	30.1811	3.5134
300	.2280	36.5536	4.1839
350	.2643	42.3625	4.8501

TABLE: 8

SOLUTION: 0.3% NATROSOL-250 HR

DENSITY OF SOLUTION: 1.01507 gm/cm^3

DATA FOR CAPILLARY A:

ΔP, PSIG	W, gm/sec.	$\frac{8\langle U\rangle}{D} \times 10^{-4}$, sec^{-1}	τ_w, gm_f/cm^2
10	.1949	.9977	0.4617
16	.3794	1.9418	0.7175
20	.5255	2.6896	0.8818
26	.7144	3.6561	1.1246
32	.9429	4.8256	1.3528
40	1.1042	5.6511	1.6749

DATA FOR CAPILLARY B:

ΔP, PSIG	W, gm/sec.	$\frac{8\langle U\rangle}{D} \times 10^{-4}$, sec^{-1}	τ_w, gm_f/cm^2
20	.0925	1.4916	.6204
40	.2448	3.9453	1.2123
50	.3270	5.2705	1.5014
60	.4125	6.6485	1.7852
80	.5773	9.3043	2.3414
100	.7586	12.2259	2.8723

DATA FOR CAPILLARY C:

ΔP, PSIG	W, gm/sec.	$\frac{8\langle U\rangle}{D} \times 10^{-4}$, sec^{-1}	τ_w, gm_f/cm^2
50	.0722	3.1141	1.0973
80	.1355	5.8420	1.7407
120	.2175	9.3799	2.5889
150	.2586	11.1474	3.2268
200	.4031	17.3788	4.2365
250	.5083	21.9130	5.2459

DATA FOR CAPILLARY D:

ΔP, PSIG	W, gm/sec.	$\frac{8\langle U\rangle}{D} \times 10^{-4}$, sec^{-1}	τ_w, gm_f/cm^2
80	.0906	5.7991	1.5582
150	.2029	12.9893	2.8803
200	.2846	18.2153	3.8036
260	.3737	23.9231	4.8975
320	.4633	29.6521	5.9705
350	.5089	32.5750	6.4980

TABLE: 9

SOLUTION: 0.4% NATROSOL-250 HR

DENSITY OF SOLUTION: 1.0153 gm/cm^3

DATA FOR CAPILLARY A:

ΔP, PSIG	W, gm/sec.	$\frac{8\langle U\rangle}{D} \times 10^{-4}$, sec^{-1}	τ_w, gm_f/cm^2
10	.1236	.6394	.4623
16	.2708	1.4013	.7216
20	.3714	1.9216	.8916
26	.5356	2.7714	1.1416
32	.7258	3.7555	1.3823
40	.9537	4.9345	1.6970

DATA FOR CAPILLARY B:

ΔP, PSIG	W, gm/sec.	$\frac{8\langle U\rangle}{D} \times 10^{-4}$, sec^{-1}	τ_w, gm_f/cm^2
20	0.0639	1.0352	.6210
40	0.1835	2.9696	1.2188
50	0.2458	3.9763	1.5137
60	0.3108	5.0277	1.8055
80	.4794	7.7556	2.3700
100	.6122	9.9035	2.9308

DATA FOR CAPILLARY C:

ΔP, PSIG	W, gm/sec.	$\frac{8\langle U\rangle}{D} \times 10^{-4}$, sec^{-1}	τ_w, gm_f/cm^2
50	.0562	2.4273	1.0981
80	.1112	4.8063	1.7441
120	.1747	7.5502	2.6005
150	.2126	9.1876	3.2418
200	.2602	11.2436	4.3126

DATA FOR CAPILLARY D:

ΔP, PSIG	W, gm/sec.	$\frac{8\langle U\rangle}{D} \times 10^{-4}$, sec^{-1}	τ_w, gm_f/cm^2
80	0.0798	5.0855	1.7314
150	.1623	10.3348	3.2173
200	.1999	12.7319	4.2795
260	.2138	13.6099	5.5693
320	.2272	14.4647	6.8588

DATA FOR CAPILLARY E:

ΔP, PSIG	W, gm/sec.	$\frac{8\langle U\rangle}{D} \times 10^{-4}$, sec^{-1}	τ_w, gm_f/cm^2
100	.0343	5.4914	1.4519
150	.0572	9.1662	2.1690
200	.0759	12.1632	2.8848
260	.0946	15.1644	3.7444
350	.1398	22.4001	5.0103

APPENDIX II

SAMPLE CALCULATIONS

A. The calculation of shear stress versus shear rate for the flow of 1.0% Natrosol-250 G Solution.

Density of the solution at 25° C = 1.0169 gm/c.c.

The diameter of the capillary tube = 0.0578 cm.

Pressure drop across the capillary tube = 40.0 p sig.

Flow rate of the solution = 0.5321 gm/sec.

$$\text{Shear Rate} = \frac{8\langle U\rangle}{D} = \frac{32\ W}{\pi\rho D^3}$$

$$= \frac{32 \times 0.5321}{3.1428 \times 1.0169 \times (0.0578)^3} \ \text{sec}^{-1}$$

$$= 2.7590 \times 10^4 \ \text{sec}^{-1}$$

$$\text{Shear Stress} = r_H \left(-\frac{dp'}{dx}\right)$$

From Equation (E-11) in Chapter III,

$$\left(-\frac{dp'}{dx}\right) = \frac{40.0 \times 70.3324}{22.96} + \frac{5.5+22.96}{22.96} - \frac{1.12 \times 1.0169 \times 3.9542 \times 10^4}{22.96 \times 980}$$

$$= (122.5303 + 1.2395 - 2.0012)\ gm_f/cm^3$$

$$= 121.7686\ gm_f/cm^3$$

$$\tau_w = r_H \left(-\frac{dp'}{dx}\right) = 0.0145 \times 121.7675\ gm_f/cm^2$$

$$= 1.7656\ gm_f/cm^2$$

B. Calculation of the effective slip velocity at a shear stress of 1.7656 gm_f/cm^2

The diameter of the capillary tube = 0.0578 cm

The critical shear stress for 1.0% Natrosol-250 G (Figure 7) = 8.0 gm_f/cm^2

From the equation (B-6) in Chapter III

$$U_w = \frac{\alpha'}{D} (\tau_w - \tau_c)$$

α' is obtained from the figure 10.

Therefore, $U_w = \frac{.2799}{0.0578} (1.7656-8.0)$ cm/sec

$= - 30.1903$ cm/sec.

C. Calculation of the anomalous layer thickness for 1.0% Natrosol-250 G Solution at a Shear Stress of 1.7656 gm_f/cm^2.

From Equation (D-5) in Chapter III

$$\delta = -\frac{U_w}{f(\tau_w)}$$

From Equation (D-6) in Chapter III

$$f(\tau_w) = \frac{1+3n'}{4n'} \left\{\frac{8(\langle U \rangle - U_w)}{D}\right\}$$

The flow behavior index n' is obtained from the 1.0% Natrosol-250 G Solution Curve in Figure 11.

Therefore, $\frac{1+3n'}{4n'} = \frac{1+3\times0.75}{4\times0.75} = 1.0833$

$$f(\tau_w) = 1.0833 \times 3.1670 \times 10^4 \text{ sec}^{-1}$$

$$= 3.4319 \times 10^4 \text{ sec}^{-1}$$

The true shear rate value is also obtained from the figure 11.

So, $\delta = -\frac{U_w}{f(\tau_w)} = \frac{30.1903}{3.4319\times10^4}$ cm

$$= 8.7969 \times 10^{-4} \text{ cm.}$$